LETTER

https://doi.org/10.1038/s41586-019-1002-0

TRAIP is a master regulator of DNA interstrand crosslink repair

R. Alex Wu[1,8], Daniel R. Semlow[1,8], Ashley N. Kamimae-Lanning[2], Olga V. Kochenova[1], Gheorghe Chistol[1], Michael R. Hodskinson[2], Ravindra Amunugama[1], Justin L. Sparks[1], Meng Wang[2,3], Lin Deng[1,4,5], Claudia A. Mimoso[1], Emily Low[1], Ketan J. Patel[2,6] & Johannes C. Walter[1,7]*

Cells often use multiple pathways to repair the same DNA lesion, and the choice of pathway has substantial implications for the fidelity of genome maintenance. DNA interstrand crosslinks covalently link the two strands of DNA, and thereby block replication and transcription; the cytotoxicity of these crosslinks is exploited for chemotherapy. In *Xenopus* egg extracts, the collision of replication forks with interstrand crosslinks initiates two distinct repair pathways. NEIL3 glycosylase can cleave the crosslink[1]; however, if this fails, Fanconi anaemia proteins incise the phosphodiester backbone that surrounds the interstrand crosslink, generating a double-strand-break intermediate that is repaired by homologous recombination[2]. It is not known how the simpler NEIL3 pathway is prioritized over the Fanconi anaemia pathway, which can cause genomic rearrangements. Here we show that the E3 ubiquitin ligase TRAIP is required for both pathways. When two replisomes converge at an interstrand crosslink, TRAIP ubiquitylates the replicative DNA helicase CMG (the complex of CDC45, MCM2–7 and GINS). Short ubiquitin chains recruit NEIL3 through direct binding, whereas longer chains are required for the unloading of CMG by the p97 ATPase, which enables the Fanconi anaemia pathway. Thus, TRAIP controls the choice between the two known pathways of replication-coupled interstrand-crosslink repair. These results, together with our other recent findings[3,4] establish TRAIP as a master regulator of CMG unloading and the response of the replisome to obstacles.

ICLs are formed by chemotherapeutics and endogenous aldehydes[5,6]. The classic ICL repair pathway involves 22 'FANC' proteins, defects in which cause Fanconi anaemia, a disease characterized by bone marrow failure and a predisposition to cancers[6]. Previously we have shown that, in *Xenopus* egg extracts, the Fanconi anaemia pathway is initiated by the convergence of two replication forks on an ICL, which triggers the unloading of the CMG helicase by p97[1,2,7,8]. CMG unloading involves polyubiquitylation of its MCM7 subunit[8], enabling fork reversal and ICL unhooking via nucleolytic incisions that convert the ICL into a double-strand break[2,9,10] (Fig. 1a, left branch). An alternative unhooking mechanism acts on a subset of ICLs[1] (Fig. 1a, right branch). In this alternative pathway the NEIL3 DNA glycosylase cleaves one of the two *N*-glycosyl bonds comprising the ICL, which avoids the formation of a double-strand break but generates an abasic site that is bypassed by translesion synthesis polymerases. Although both pathways are triggered by fork convergence, only the Fanconi anaemia pathway requires CMG unloading[1]. In mammals, mutations in FANC genes cause stronger phenotypes than mutations in *NEIL3*[11–14]. Therefore, cells may first attempt the simpler NEIL3 pathway, but seem to rely more heavily on the versatile Fanconi anaemia pathway for survival. Given the different mutagenic potentials of these two mechanisms, it is crucial to understand how the choice between them is governed.

A critical gap in our knowledge concerns the identity of the E3 ubiquitin ligase that ubiquitylates CMG at ICLs to activate CMG unloading and entry into the Fanconi anaemia pathway. The RING E3 ligase TRAIP (TRAF-interacting protein) is essential for cell proliferation[15], and hypomorphic TRAIP mutations cause microcephalic primordial dwarfism[16]. Because TRAIP associates with ICL-containing chromatin[17] and its knockdown sensitizes cells to mitomycin C[18], we asked whether TRAIP promotes CMG unloading at ICLs. We used *Xenopus* egg extracts to replicate a plasmid containing a site-specific cisplatin-ICL ($pICL^{Pt}$) (Extended Data Fig. 1a). In mock-depleted extract, forks converged on the ICL and stalled, generating a discrete 'slow-figure-8' intermediate that was converted to a 'fast-figure-8' species upon CMG unloading[9] (Fig. 1b, lanes 1–3, Extended Data Fig. 1b; for gel source data, see Supplementary Fig. 1). Notably, the depletion of TRAIP (Extended Data Fig. 2a) caused an accumulation of the slow-figure-8 species (Fig. 1b, lanes 11–15), the same defect as that observed when CMG unloading was blocked with p97 inhibitor[1] (p97i; Fig. 1b, lanes 6–10). Wild-type recombinant *Xenopus* TRAIP (rTRAIP), purified from bacteria or insect cells (Extended Data Fig. 2b, c), restored the formation of the fast-figure-8 species (Fig. 1b, Extended Data Fig. 2d–h).

These results suggested that TRAIP promotes CMG ubiquitylation and unloading. Consistent with this idea, we found that TRAIP was required for the dissociation of CDC45 and MCM7 (two subunits of CMG) from $pICL^{Pt}$ (Fig. 1c), and for efficient loss of the CMG footprint at ICLs (Extended Data Fig. 3a, b). Loss of the CMG footprint did not require FANCM or ATR signalling (Extended Data Fig. 3c–f), two factors that mediate fork traverse at ICLs[19,20]. In addition, MCM7 ubiquitylation was dependent on TRAIP (Fig. 1c). This effect was more evident when CMG unloading was blocked with p97i (Fig. 1d). Consistent with CMG unloading being required for fork reversal and incisions at an ICL[9], TRAIP was also required for fork reversal and for error-free repair of the lesion (Fig. 1e, f). rTRAIP(R18C)—which harbours a RING-domain mutation (Arg18 to Cys) that is associated with primordial dwarfism[16]—was defective for fast-figure-8 formation, MCM7 ubiquitylation and unloading, fork reversal, and ICL repair (Fig. 1b–f, Extended Data Fig. 2b–h). The low activity of rTRAIP(R18C) probably results from a combination of modest defects both in chromatin recruitment (Fig. 1c, d) and in E3 ubiquitin ligase activity (see below). Our previous conclusion that BRCA1 is required for CMG unloading[21] resulted from the inadvertent depletion of TRAIP with BRCA1 antiserum (Extended Data Fig. 3i–n). We conclude that TRAIP is required for MCM7 ubiquitylation and CMG unloading in the Fanconi anaemia ICL-repair pathway.

Consistent with CMG unloading at ICLs requiring fork convergence[7], MCM7 ubiquitylation was also found to depend on convergence (Fig. 2a). Thus, either TRAIP is recruited de novo when CMGs converge on an ICL, or it travels with the replisome but only ubiquitylates CMG upon fork convergence. In agreement with the latter

[1]Department of Biological Chemistry and Molecular Pharmacology, Harvard Medical School, Boston, MA, USA. [2]MRC Laboratory of Molecular Biology, Cambridge Biomedical Campus, Cambridge, UK. [3]Department of Haematology, University of Cambridge, Cambridge, UK. [4]Department of Pediatric Oncology, Dana-Farber Cancer Institute, Boston, MA, USA. [5]Department of Cell Biology, Harvard Medical School, Boston, MA, USA. [6]Department of Medicine, University of Cambridge, Addenbrooke's Hospital, Cambridge, UK. [7]Howard Hughes Medical Institute, Boston, MA, USA. [8]These authors contributed equally: R. Alex Wu, Daniel R. Semlow. *e-mail: johannes_walter@hms.harvard.edu

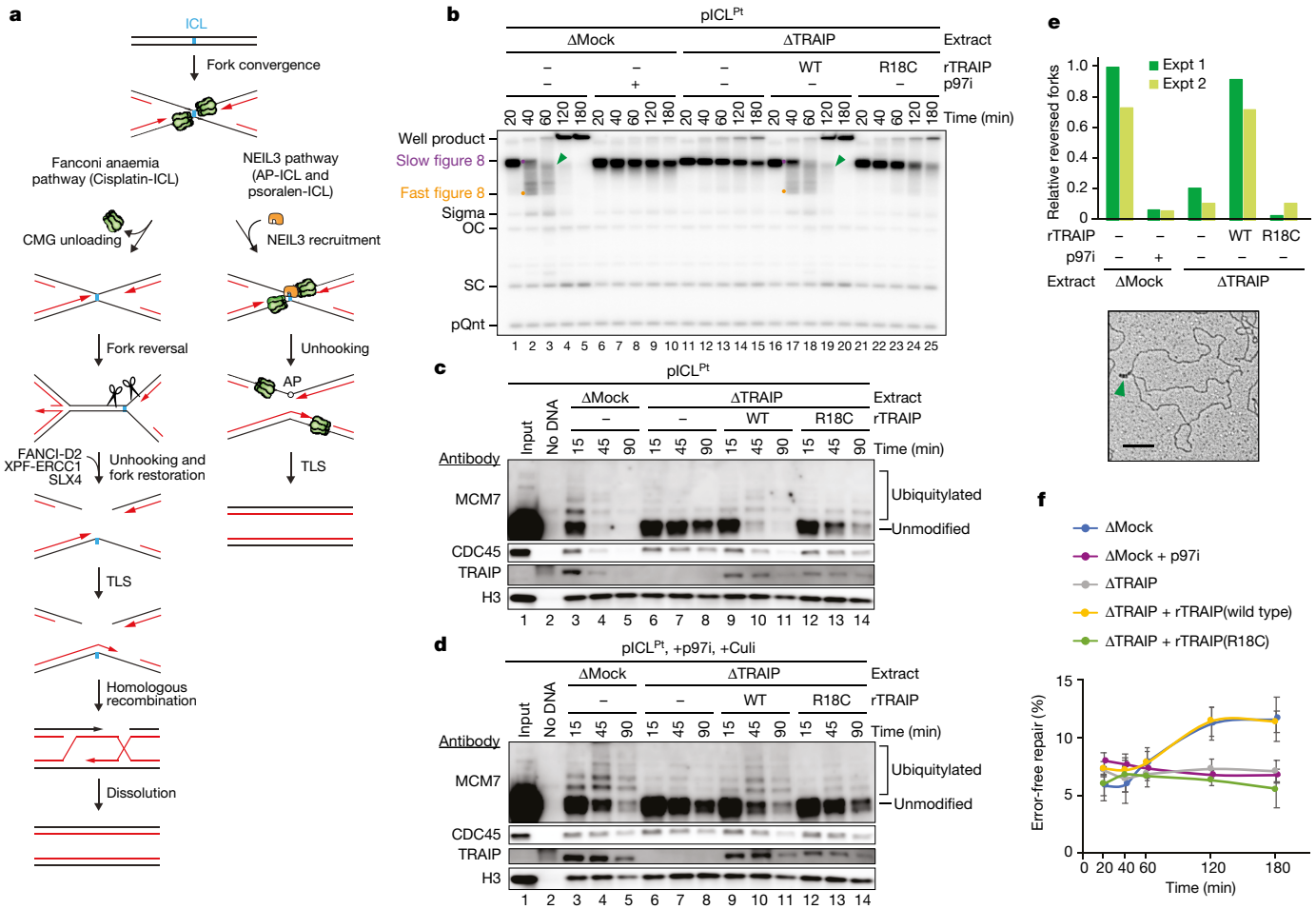

Fig. 1 | CMG unloading at ICLs requires the E3 ubiquitin ligase TRAIP. **a**, Models of ICL repair by the Fanconi anaemia (left branch) and NEIL3 (right branch) pathways. AP, abasic site; TLS, translesion DNA synthesis. **b**, pICL^{Pt} was replicated in *Xenopus* egg extracts containing [α-^{32}P]dATP. Replication intermediates were resolved by native agarose gel electrophoresis and visualized by autoradiography. Wild-type rTRAIP, rTRAIP(R18C) and p97 inhibitor NMS-873 (p97i) were added as indicated. Purple dot, slow-figure-8 species; orange dot, fast-figure-8 species; green arrows, reversed fork; OC, open circular; SC, supercoiled; pQnt, undamaged control plasmid. See Extended Data Fig. 1b for description of well products, reversed forks and sigmas. For TRAIP levels in extracts, see Extended Data Fig. 2d. Seven independent experiments. **c**, **d**, Analysis of proteins associated with pICL^{Pt} during replication in the indicated extracts in the absence (**c**) or presence (**d**) of p97i and Cullin RING ubiquitin ligase inhibitor MLN4924 (Culi). Culi was added to eliminate ubiquitylation by CRL2^{LRR1} (see Extended Data Fig. 4d). For TRAIP levels in extracts, see Extended Data Fig. 2i. Residual MCM7 ubiquitylation in the presence of rTRAIP(R18C) was observed in eight independent experiments (for example, Fig. 3c). Histone H3, recovery control. Three independent experiments (**c**), two independent experiments (**d**). **e**, Top, pICL^{Pt} was replicated for 90 min in the indicated extracts, and the relative abundance of reversed forks, as determined by electron microscopy, was quantified. Values, normalized to the mock-depleted extract, are shown for two independent experiments. Bottom, representative electron micrograph of a reversed fork (green arrow) from TRAIP-depleted extract supplemented with wild-type rTRAIP. For TRAIP levels in extracts, see Extended Data Fig. 3g. Scale bar, 200 nm. **f**, Error-free repair as measured by regeneration of a SapI restriction site coinciding with the ICL. The basal SapI cutting (approximately 7%) is due to contaminating undamaged plasmid[10]. Data are mean ± s.e.m. from three independent experiments. For TRAIP levels in extracts, see Extended Data Fig. 3h.

scenario, TRAIP associated with the undamaged control plasmid (pCtrl) at levels similar to those seen on pICL (Fig. 2b, compare lanes 2 and 5), and in mammalian cells TRAIP localizes to DNA replication forks in the absence of exogenous insults[16,18]. Both replication licensing and initiation were essential to recruit TRAIP to chromatin (Extended Data Fig. 4a, b). TRAIP contains a conserved, C-terminal PIP box (PIP, PCNA-interacting peptide; PCNA, proliferating cell nuclear antigen)[18], which suggests that PCNA might recruit TRAIP to replication forks. However, a mutated TRAIP that lacks the PIP box (TRAIP(ΔPIP)) still suppresses hypersensitivity to mitomycin C[18]. Accordingly, recombinant *Xenopus* TRAIP(ΔPIP) suppressed the accumulation of slow-figure-8 species (Extended Data Fig. 2b, g, h). TRAIP therefore travels with the replisome but ubiquitylates CMG only after fork convergence at an ICL, independently of its PIP box.

CMG unloading during replication termination involves the polyubiquitylation of MCM7 by CRL2^{LRR1} (refs [22,23]), and this process does not require TRAIP (Extended Data Fig. 4d, e). Conversely, MCM7 ubiquitylation at ICLs does not require CRL2^{LRR1} (Extended Data Fig. 4f–h). Unlike replication termination, ICL repair involved TRAIP-dependent ubiquitylation of MCM2, MCM3, MCM4, MCM6, and MCM7, and the partial ubiquitylation of CDC45, but almost no detectable ubiquitylation of PSF1 and PSF3 (Fig. 2c, Extended Data Fig. 5a, b) or other replisome-associated factors (Extended Data Fig. 5c). Wild-type rTRAIP produced a generally similar ubiquitylation pattern on purified recombinant CMG (Fig. 2d, Extended Data Fig. 5d), consistent with the direct ubiquitylation of CMG by TRAIP in extracts. rTRAIP(R18C) was partially compromised for in vitro ubiquitylation (Fig. 2d, Extended Data Fig. 5e). TRAIP-dependent ubiquitin chains on CMG were largely insensitive to treatment with chain-specific deubiquitylating enzymes and the addition of ubiquitin lysine mutants that restrict the formation of specific chain types (Extended Data Fig. 5f–h). Thus, in contrast to CRL2^{LRR1}, which deposits K48-linked ubiquitin

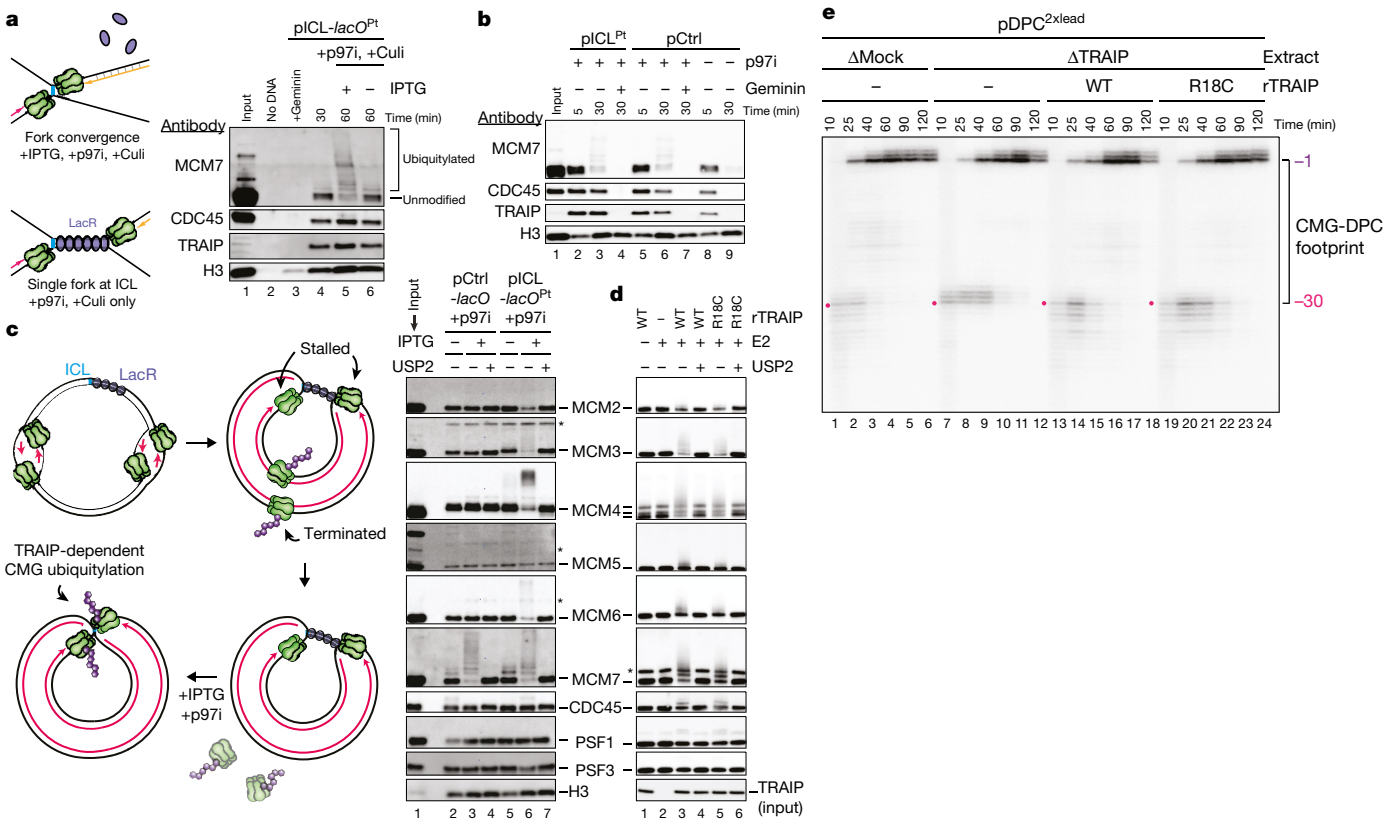

Fig. 2 | TRAIP ubiquitylates CMGs that have converged at ICLs. **a**, Left, experimental scheme. Plasmid containing an ICL flanked by 48 copies of the *lac* operator (*lacO*) (pICL-*lacO*^{Pt}) was incubated with Lac repressor (LacR) before replication in undepleted egg extract. After 30 min, the addition of isopropyl β-D-1-thiogalactopyranoside (IPTG) dissociated LacR and enabled fork convergence. Right, pICL-*lacO*^{Pt} was recovered and analysed for the indicated proteins using immunoblotting. Culi suppressed CRL2^{LRR1}-dependent ubiquitylation. Two independent experiments. **b**, Chromatin-associated proteins during replication of pICL^{Pt} or pCtrl in undepleted extract in the presence or absence of the licensing inhibitor Geminin and p97i. Five independent experiments. **c**, Left, after CRL2^{LRR1}-dependent unloading of CMGs that underwent termination on plasmids with multiple initiation events (see Extended Data Fig. 4d), release of the LacR array with IPTG leads to convergence of forks at the ICL, enabling analysis of TRAIP-specific ubiquitylation. Right, analysis of proteins associated with pICL-*lacO*^{Pt} during replication in the presence of p97i. MCM2 ubiquitylation was inferred from the increase in unmodified MCM2 upon USP2 treatment, which was used to remove all ubiquitin modifications. Asterisks, non-specifically detected proteins. Two independent experiments. **d**, Analysis of rCMG subunits incubated with rTRAIP in the presence of ubiquitin, E1 activating enzyme, UbcH5a, UbcH5b, and UbcH5c E2 conjugating enzymes, and ATP. MCM4 was present in its full-length and as degradation products. Asterisk, non-specifically detected protein. Five independent experiments. **e**, Nascent strand analysis of pDPC$^{2\times lead}$ (DPC, DNA–protein crosslink) replicated in the indicated extracts. Red dot, combined footprint of CMG and the DNA–protein crosslink in the presence of TRAIP. For TRAIP levels in extracts, see Extended Data Fig. 4c. Four independent experiments.

chains during termination[22], TRAIP can deposit ubiquitin chains that seem to be heterotypically linked and/or branched.

We recently found that collision of a replication fork with a DNA–protein crosslink leads to TRAIP-dependent ubiquitylation of the crosslink[3]. Here we observed that, upon TRAIP depletion, the leading strand advanced two nucleotides closer to a DNA–protein crosslink, and both wild-type rTRAIP and rTRAIP(R18C) restored the original footprint (Fig. 2e). By contrast, no such effect was seen at ICLs (Extended Data Fig. 3a), which indicates that TRAIP clashes only with bulky obstacles. Thus, TRAIP seems to associate with the leading edge of the replisome, where it non-specifically ubiquitylates lysine residues on proteinaceous obstacles encountered ahead of the fork—including on ubiquitin itself—resulting in complex ubiquitin chains that are not dominated by a single linkage type.

Unlike cisplatin-ICLs, psoralen-ICLs and AP-ICLs (apurinic/apyrimidinic ICLs, formed between an abasic site in one strand and an adenosine in the other strand) are unhooked by NEIL3 independently of CMG unloading[1]. However, we found that MCM7 was ubiquitylated with similar kinetics at both AP-ICLs and cisplatin-ICLs (Extended Data Fig. 6a). We therefore asked whether AP-ICL repair requires TRAIP. In mock-depleted extract, slow-figure-8 species that were generated when forks converged on an AP-ICL were converted directly into open circular and supercoiled products by NEIL3-dependent unhooking[1] (Fig. 3a; for schematic of pICL^{AP} repair intermediates see Extended Data Fig. 1c). Unlike p97 inhibition—which had no effect on AP-ICL replication[1] (Extended Data Fig. 6b, lanes 26–30)—TRAIP immunodepletion caused a marked accumulation of slow-figure-8 species and a strong reduction in open circular and supercoiled plasmids (Fig. 3a). Furthermore, TRAIP depletion greatly reduced AP-ICL repair (Fig. 3b). The addition of wild-type rTRAIP, purified from bacteria or insect cells, fully reversed these defects (Fig. 3a, b, Extended Data Fig. 6e, f). rTRAIP(R18C) also mostly reversed these defects, suggesting that lower levels of ubiquitylation are needed to support AP-ICL repair compared with cisplatin-ICL repair (Fig. 3a, b, Extended Data Fig. 6e). Thus, TRAIP promotes AP-ICL repair independently of CMG unloading.

We postulated that TRAIP-dependent CMG ubiquitylation recruits NEIL3 to converged forks. Because endogenous NEIL3 on chromatin was undetectable by immunoblotting, we supplemented extract with Flag-tagged recombinant NEIL3 (rNEIL3) and examined its chromatin binding using Flag antibody. rNEIL3 recovery was abolished by Geminin, demonstrating that rNEIL3 binding is replication-dependent (Extended Data Fig. 6a). We detected more rNEIL3 on pICL^{Pt} than on pICL^{AP} (Extended Data Fig. 6a), probably because NEIL3 becomes trapped on chromatin when it cannot unhook the ICL (Extended Data Fig. 7a, b). pICL^{Pt} was therefore used for subsequent

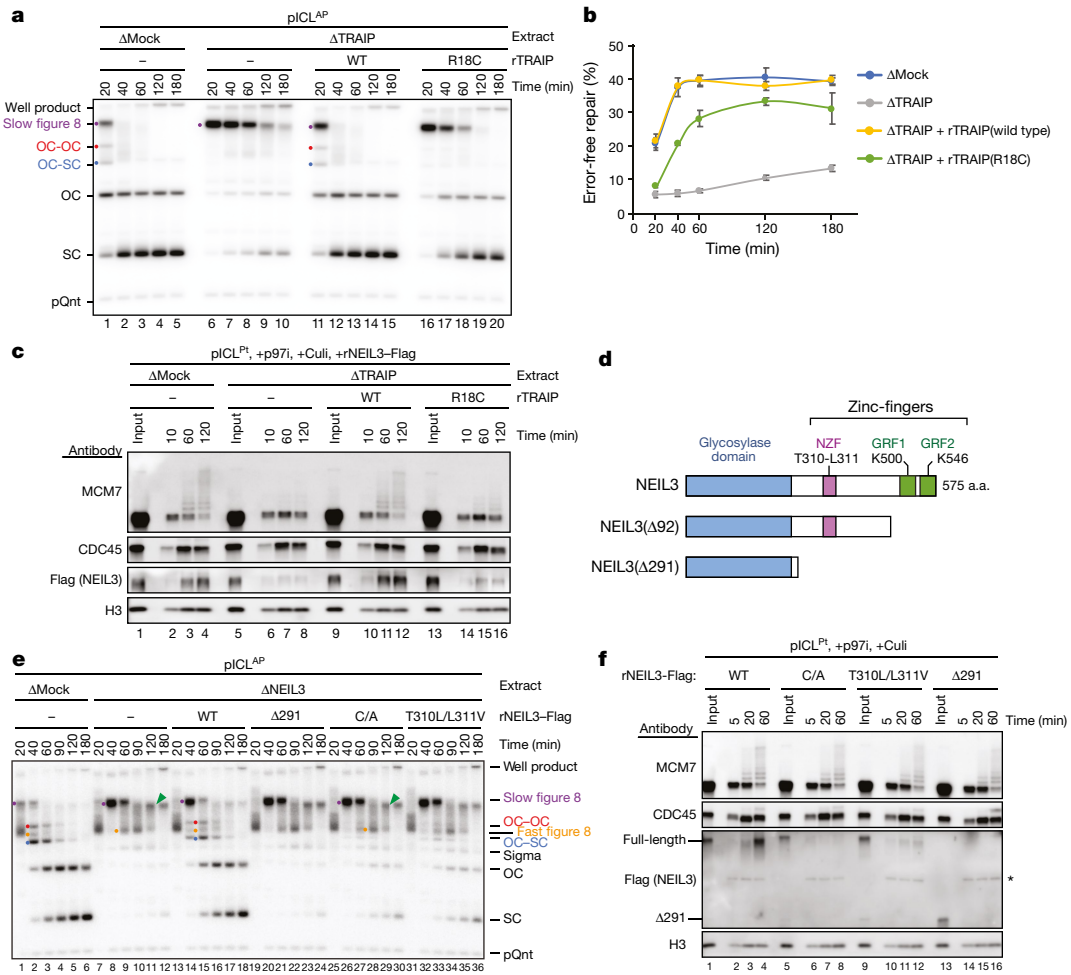

Fig. 3 | TRAIP promotes NEIL3-dependent ICL repair. **a**, pICL^{AP} was replicated in the indicated extracts and analysed as in Fig. 1b. Red dot, OC–OC catenane; blue dot, OC–SC catenane. For TRAIP levels in extracts, see Extended Data Fig. 6c. Five independent experiments. **b**, Error-free repair of pICL^{AP} was quantified as in Fig. 1f. Data are mean ± s.e.m. from three independent experiments. For TRAIP levels in extracts, see Extended Data Fig. 6d. **c**, **f**, Analysis of proteins associated with pICL^{Pt} during replication in the indicated extracts (**c**) or undepleted extract (**f**) in the presence of p97i and Culi. Asterisk, non-specifically detected protein. Four independent experiments (**c**), three independent experiments (**f**). For TRAIP levels in extracts used in **c**, see Extended Data Fig. 7c. **d**, Schematic of *Xenopus* NEIL3 proteins. **e**, pICL^{AP} was replicated in the indicated extracts and analysed as in Fig. 1b. ICL unhooking was estimated by quantifying the open circular and supercoiled signals normalized to pQnt. For NEIL3 levels in extracts, see Extended Data Fig. 8c. Three independent experiments.

NEIL3-recruitment assays. We also found that the depletion of TRAIP strongly reduced the association of rNEIL3 with pICL^{Pt} (Fig. 3c, lanes 1–8). Recombinant wild-type TRAIP fully rescued and rTRAIP(R18C) partially rescued this defect (Fig. 3c). Our data suggest that TRAIP-dependent CMG ubiquitylation is required to recruit NEIL3 for the unhooking of ICLs. Consistent with this model, delaying the unloading of CMG extends the window of time during which NEIL3 can unhook an AP-ICL (Extended Data Fig. 7d, e).

NEIL3 contains three zinc-finger motifs C-terminal to its glycosylase domain[24] (Fig. 3d). NEIL3 lacking the entire C-terminal region (rNEIL3(Δ291)) retained glycosylase activity (Extended Data Fig. 8a) but failed to unhook pICL^{AP} (Fig. 3e) or bind pICL in extract (Fig. 3f), which suggests that one or more of the zinc-fingers helps to recruit NEIL3 to stalled forks. We found that the NPL4-type zinc-finger (NZF) of NEIL3 binds monoubiquitin, and that this interaction is dependent on a conserved NZF TL motif (Extended Data Fig. 8b), as seen for other NZFs[25]. Notably, pICL^{AP} unhooking was reduced more than twofold by substitution of the TL motif (rNEIL3(T310L/L311V)) and fourfold by substitutions of zinc-coordinating cysteines in the NZF (rNEIL3-NZF(C/A); Fig. 3e). Consistent with this observation, rNEIL3-NZF(C/A) and rNEIL3(T310L/L311V) showed diminished binding to pICL (Fig. 3f). The other two NEIL3 zinc-fingers resemble the 'GRF' zinc-finger of APE2 endonuclease, which binds single-stranded (ss)DNA[26]. We found that GRF1 and GRF2 each bound specifically to ssDNA (Extended Data Fig. 8d, e), and point mutations that disrupted this binding compromised the association of NEIL3 with chromatin and its ability to support AP-ICL unhooking (Extended Data Fig. 8f–h). Our data suggest that NEIL3 binds to converged CMGs through cooperation of its NZF (which recognizes ubiquitylated CMG) and its GRFs (which recognize ssDNA, possibly on the lagging strand template) (Extended Data Fig. 8i).

In *Xenopus* egg extracts, AP-ICLs and psoralen-ICLs are processed almost exclusively by NEIL3, but in its absence they are unhooked by the Fanconi anaemia pathway[1]. The question arises as to how the NEIL3 pathway is prioritized over the Fanconi anaemia pathway. Notably, rTRAIP(R18C), which forms only short ubiquitin chains on MCM7 (Fig. 1c, d, 3c), showed barely detectable activity in cisplatin-ICL repair (Fig. 1b, f) while promoting robust AP-ICL repair (Fig. 3a, b). These observations suggest that short ubiquitin chains might be sufficient to support the NEIL3 pathway but not the Fanconi anaemia pathway. Consistent with this hypothesis, ubiquitin that lacks lysines (Ub(K0))—and therefore cannot undergo polyubiquitylation—greatly stabilized pICL^{Pt} slow-figure-8 intermediates (which is indicative of defective p97-dependent CMG unloading), while having only a modest effect on the disappearance of pICL^{AP} slow-figure-8 species, which reflects NEIL3 unhooking (Fig. 4a). As expected, Ub(K0) reduced the length of ubiquitin chains formed on MCM7 (Fig. 4b, red bar). Consistent with its modest effect on the unhooking of AP-ICLs, Ub(K0) did not affect the recruitment of NEIL3 to chromatin (Fig. 4b). The data suggest that short ubiquitin chains on CMG are sufficient to recruit NEIL3. If the ICL cannot be cleaved by NEIL3—as in the case of cisplatin-ICLs—the chains continue to grow, leading to p97-dependent CMG unloading (Fig. 4c). Consistent with the redundancy between the Fanconi anaemia pathway and the NEIL3 pathway for the repair of certain ICLs in mammalian cells, both had to be eliminated in order to observe hypersensitivity to psoralen-ICLs, whereas removal of the Fanconi anaemia pathway alone sensitized HAP1 cells to cisplatin (Fig. 4d, Extended Data Fig. 9a–d). A synthetic interaction between the NEIL3 pathway and the Fanconi anaemia pathway was also observed in the CH12 B cell line (Extended Data Fig. 9e–g). Whether the NEIL3 pathway is prioritized in cells, as seen in extracts, remains to be determined.

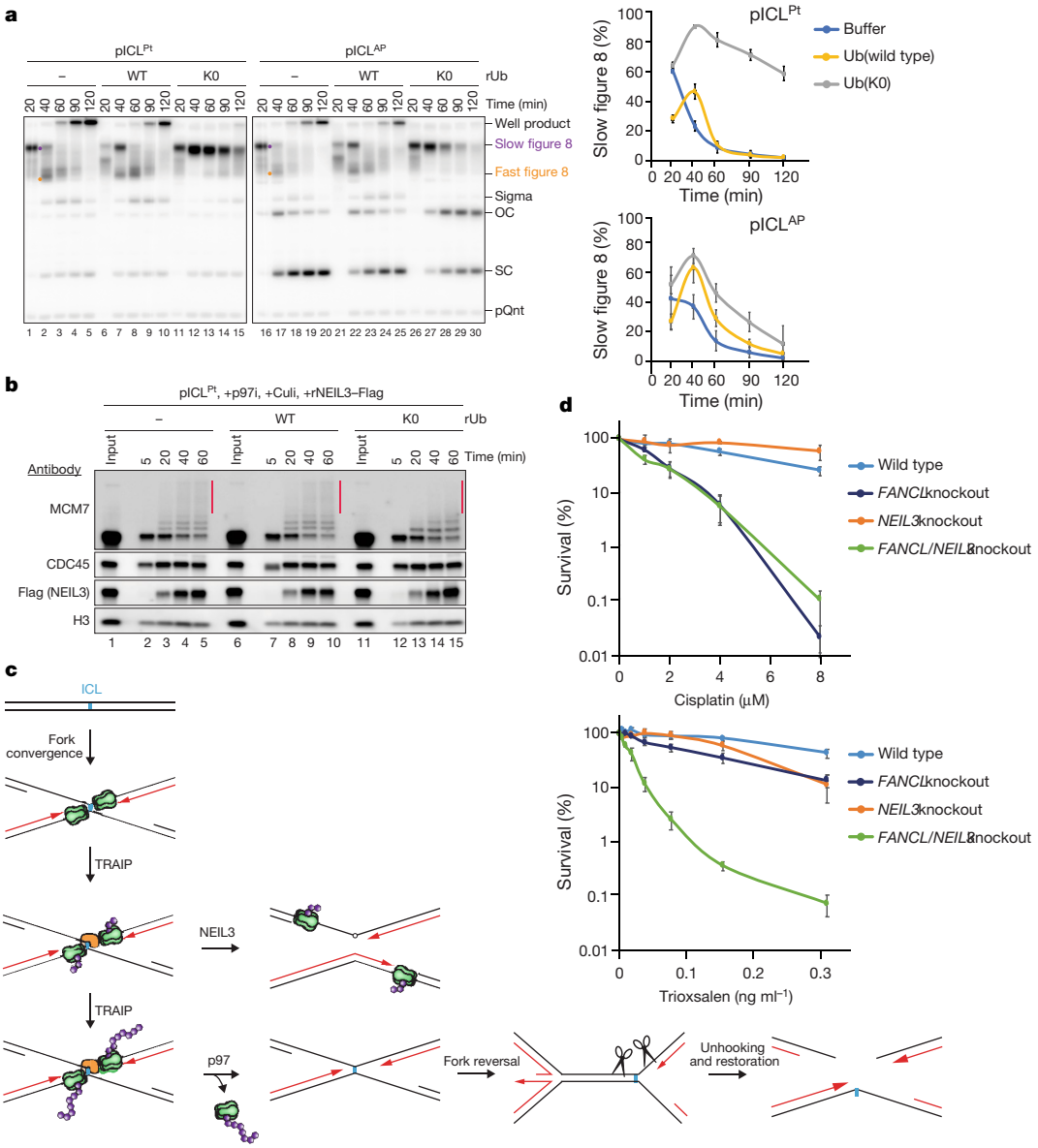

Fig. 4 | The MCM7 ubiquitin chain length influences the choice of ICL repair pathway. a, Left, replication of pICL^{Pt} or pICL^{AP} in undepleted extract supplemented with buffer, wild-type Ub or Ub(K0) was analysed as in Fig. 1b. Right, slow-figure-8 structures quantified as a percentage of total replication products. Note that wild-type Ub and Ub(K0) delayed replication by about 20 minutes. Data are mean ± s.e.m. from three independent experiments. **b**, Proteins associated with pICL^{Pt} during replication in undepleted extract in the presence of p97i and Culi and wild-type Ub or Ub(K0), as indicated. The red bar indicates longer ubiquitin chains sensitive to Ub(K0) addition. Four independent experiments. **c**, Model for hierarchical activation of the NEIL3 and Fanconi anaemia pathways by TRAIP. Green, CMG helicase; purple, ubiquitin; orange, NEIL3. **d**, Clonogenic survival of wild-type, as well as *FANCL*-knockout, *NEIL3*-knockout or *FANCL*/*NEIL3*-knockout HAP1 cells after exposure to cisplatin (top) or trioxsalen and UVA irradiation (bottom). Data are mean ± s.e.m. from three independent experiments (cisplatin) or four independent experiments (trioxsalen).

We have shown that although TRAIP is a constitutive replisome component, it ubiquitylates CMG only upon fork convergence, and this avoids premature CMG unloading from active replisomes (Extended Data Fig. 10a, i). Given our data, the ICL sensitivity of cells that lack TRAIP[18] suggests that a substantial number of ICL repair events in cells require CMG convergence, even though a single fork may often trigger repair[19]. It is notable that TRAIP also supports replication-coupled ubiquitylation of DNA–protein crosslinks[3] (Extended Data Fig. 10a, ii). Moreover, in mitosis, TRAIP ubiquitylates stalled CMGs in the absence of fork convergence, and terminated CMGs that were not unloaded by CRL2^{LRR1} (ref. [4]) (Extended Data Fig. 10a, iii, iv). Collectively our data suggest that, in interphase, TRAIP ubiquitylates only proteins that are located ahead of the replisome. By contrast, in mitosis, TRAIP also ubiquitylates the CMG with which it associates, perhaps owing to a cyclin B1-CDK1-dependent conformational change in TRAIP. We speculate that in humans, the ubiquitylation activity associated with TRAIP(R18C) is sufficient to support the Fanconi anaemia pathway, albeit with slow kinetics; this would suppress the symptoms of Fanconi anaemia while causing a G2 delay, reduced cell proliferation and dwarfism. Consistent with this model, cells from patients with Fanconi anaemia and from patients deficient in TRAIP exhibit slow progression through G2 in the absence of exogenous crosslinking agents[6,27], and patients with Fanconi anaemia often exhibit short stature[6]. In conclusion, our results establish TRAIP as a replisome-associated E3 ubiquitin ligase that controls ICL repair-pathway choice, replisome integrity, and the response to proteinaceous replication barriers.

Online content

Any methods, additional references, Nature Research reporting summaries, source data, statements of data availability and associated accession codes are available at https://doi.org/10.1038/s41586-019-1002-0.

Received: 5 July 2018; Accepted: 1 February 2019;
Published online: 06 March 2019

1. Semlow, D. R., Zhang, J., Budzowska, M., Drohat, A. C. & Walter, J. C. Replication-dependent unhooking of DNA interstrand cross-links by the NEIL3 glycosylase. *Cell* **167**, 498–511.e14 (2016).
2. Räschle, M. et al. Mechanism of replication-coupled DNA interstrand crosslink repair. *Cell* **134**, 969–980 (2008).
3. Larsen, N. B. et al. Mechanism of replication-coupled DNA-protein crosslink proteolysis by SPRTN and the proteasome. *Mol. Cell* **73**, 574–588 (2019).
4. Deng, L. et al. Mitotic CDK promotes replisome disassembly, fork breakage, and complex DNA rearrangements. *Mol. Cell* (in the press).
5. Price, N. E., Catalano, M. J., Liu, S., Wang, Y. & Gates, K. S. Chemical and structural characterization of interstrand cross-links formed between abasic sites and adenine residues in duplex DNA. *Nucleic Acids Res.* **43**, 3434–3441 (2015).
6. Kottemann, M. C. & Smogorzewska, A. Fanconi anaemia and the repair of Watson and Crick DNA crosslinks. *Nature* **493**, 356–363 (2013).
7. Zhang, J. et al. DNA interstrand cross-link repair requires replication-fork convergence. *Nat. Struct. Mol. Biol.* **22**, 242–247 (2015).
8. Fullbright, G., Rycenga, H. B., Gruber, J. D. & Long, D. T. p97 promotes a conserved mechanism of helicase unloading during DNA cross-link repair. *Mol. Cell. Biol.* **36**, 2983–2994 (2016).
9. Amunugama, R. et al. Replication fork reversal during DNA interstrand crosslink repair requires CMG unloading. *Cell Rep.s* **23**, 3419–3428 (2018).
10. Knipscheer, P. et al. The Fanconi anemia pathway promotes replication-dependent DNA interstrand cross-link repair. *Science* **326**, 1698–1701 (2009).
11. Massaad, M. J. et al. Deficiency of base excision repair enzyme NEIL3 drives increased predisposition to autoimmunity. *J. Clin. Invest.* **126**, 4219–4236 (2016).
12. Parmar, K., D'Andrea, A. & Niedernhofer, L. J. Mouse models of Fanconi anemia. *Mutat. Res.* **668**, 133–140 (2009).
13. Sejersted, Y. et al. Endonuclease VIII-like 3 (Neil3) DNA glycosylase promotes neurogenesis induced by hypoxia-ischemia. *Proc. Natl Acad. Sci. USA* **108**, 18802–18807 (2011).
14. Torisu, K., Tsuchimoto, D., Ohnishi, Y. & Nakabeppu, Y. Hematopoietic tissue-specific expression of mouse *Neil3* for endonuclease VIII-like protein. *J. Biochem.* **138**, 763–772 (2005).
15. Chapard, C., Hohl, D. & Huber, M. The role of the TRAF-interacting protein in proliferation and differentiation. *Exp. Dermatol.* **21**, 321–326 (2012).
16. Harley, M. E. et al. TRAIP promotes DNA damage response during genome replication and is mutated in primordial dwarfism. *Nat. Genet.* **48**, 36–43 (2016).
17. Räschle, M. et al. Proteomics reveals dynamic assembly of repair complexes during bypass of DNA cross-links. *Science* **348**, 1253671 (2015).
18. Hoffmann, S. et al. TRAIP is a PCNA-binding ubiquitin ligase that protects genome stability after replication stress. *J. Cell Biol.* **212**, 63–75 (2016).
19. Huang, J. et al. The DNA translocase FANCM/MHF promotes replication traverse of DNA interstrand crosslinks. *Mol. Cell* **52**, 434–446 (2013).
20. Mutreja, K. et al. ATR-mediated global fork slowing and reversal assist fork traverse and prevent chromosomal breakage at DNA interstrand cross-links. *Cell Rep.* **24**, 2629–2642 (2018).
21. Long, D. T., Joukov, V., Budzowska, M. & Walter, J. C. BRCA1 promotes unloading of the CMG helicase from a stalled DNA replication fork. *Mol. Cell* **56**, 174–185 (2014).
22. Priego Moreno, S., Bailey, R., Campion, N., Herron, S. & Gambus, A. Polyubiquitylation drives replisome disassembly at the termination of DNA replication. *Science* **346**, 477–481 (2014).
23. Dewar, J. M., Low, E., Mann, M., Räschle, M. & Walter, J. C. $CRL2^{Lrr1}$ promotes unloading of the vertebrate replisome from chromatin during replication termination. *Genes Dev.* **31**, 275–290 (2017).
24. Liu, M. et al. Expression and purification of active mouse and human NEIL3 proteins. *Protein Expr. Purif.* **84**, 130–139 (2012).
25. Wang, B. et al. Structure and ubiquitin interactions of the conserved zinc finger domain of Npl4. *J. Biol. Chem.* **278**, 20225–20234 (2003).
26. Wallace, B. D. et al. APE2 Zf-GRF facilitates 3′-5′ resection of DNA damage following oxidative stress. *Proc. Natl Acad. Sci. USA* **114**, 304–309 (2017).
27. Dutrillaux, B., Aurias, A., Dutrillaux, A. M., Buriot, D. & Prieur, M. The cell cycle of lymphocytes in Fanconi anemia. *Hum. Genet.* **62**, 327–332 (1982).
28. Sparks, J. L. et al. The CMG helicase bypasses DNA-protein cross-links to facilitate their repair. *Cell* **176**, 167–181.e21 (2019).
29. Lebofsky, R., Takahashi, T. & Walter, J. C. DNA replication in nucleus-free *Xenopus* egg extracts. *Methods Mol. Biol.* **521**, 229–252 (2009).
30. Dewar, J. M., Budzowska, M. & Walter, J. C. The mechanism of DNA replication termination in vertebrates. *Nature* **525**, 345–350 (2015).
31. Joukov, V., Chen, J., Fox, E. A., Green, J. B. & Livingston, D. M. Functional communication between endogenous BRCA1 and its partner, BARD1, during *Xenopus laevis* development. *Proc. Natl Acad. Sci. USA* **98**, 12078–12083 (2001).
32. Walter, J. & Newport, J. Initiation of eukaryotic DNA replication: origin unwinding and sequential chromatin association of Cdc45, RPA, and DNA polymerase α. *Mol. Cell* **5**, 617–627 (2000).
33. Byun, T. S., Pacek, M., Yee, M. C., Walter, J. C. & Cimprich, K. A. Functional uncoupling of MCM helicase and DNA polymerase activities activates the ATR-dependent checkpoint. *Genes Dev.* **19**, 1040–1052 (2005).
34. Wohlschlegel, J. A., Dhar, S. K., Prokhorova, T. A., Dutta, A. & Walter, J. C. *Xenopus* Mcm10 binds to origins of DNA replication after Mcm2-7 and stimulates origin binding of Cdc45. *Mol. Cell* **9**, 233–240 (2002).
35. Pacek, M., Tutter, A. V., Kubota, Y., Takisawa, H. & Walter, J. C. Localization of MCM2-7, Cdc45, and GINS to the site of DNA unwinding during eukaryotic DNA replication. *Mol. Cell* **21**, 581–587 (2006).
36. Kochaniak, A. B. et al. Proliferating cell nuclear antigen uses two distinct modes to move along DNA. *J. Biol. Chem.* **284**, 17700–17710 (2009).
37. Rosado, I. V., Langevin, F., Crossan, G. P., Takata, M. & Patel, K. J. Formaldehyde catabolism is essential in cells deficient for the Fanconi anemia DNA-repair pathway. *Nat. Struct. Mol. Biol.* **18**, 1432–1434 (2011).
38. Budzowska, M., Graham, T. G., Sobeck, A., Waga, S. & Walter, J. C. Regulation of the Rev1-pol ζ complex during bypass of a DNA interstrand cross-link. *EMBO J.* **34**, 1971–1985 (2015).
39. Michel, M. A. et al. Assembly and specific recognition of K29- and K33-linked polyubiquitin. *Mol. Cell* **58**, 95–109 (2015).
40. Knipscheer, P., Räschle, M., Schärer, O. D. & Walter, J. C. Replication-coupled DNA interstrand cross-link repair in *Xenopus* egg extracts. *Methods Mol. Biol.* **920**, 221–243 (2012).
41. Graham, T. G., Walter, J. C. & Loparo, J. J. Two-stage synapsis of DNA ends during non-homologous end joining. *Mol. Cell* **61**, 850–858 (2016).
42. Hemsley, A., Arnheim, N., Toney, M. D., Cortopassi, G. & Galas, D. J. A simple method for site-directed mutagenesis using the polymerase chain reaction. *Nucleic Acids Res.* **17**, 6545–6551 (1989).
43. Trowitzsch, S., Bieniossek, C., Nie, Y., Garzoni, F. & Berger, I. New baculovirus expression tools for recombinant protein complex production. *J. Struct. Biol.* **172**, 45–54 (2010).
44. Ilves, I., Petojevic, T., Pesavento, J. J. & Botchan, M. R. Activation of the MCM2-7 helicase by association with Cdc45 and GINS proteins. *Mol. Cell* **37**, 247–258 (2010).
45. Liu, M. et al. The mouse ortholog of NEIL3 is a functional DNA glycosylase in vitro and in vivo. *Proc. Natl Acad. Sci. USA* **107**, 4925–4930 (2010).
46. Franken, N. A., Rodermond, H. M., Stap, J., Haveman, J. & van Bree, C. Clonogenic assay of cells in vitro. *Nat. Protoc.* **1**, 2315–2319 (2006).
47. Vos, J. M. & Hanawalt, P. C. Processing of psoralen adducts in an active human gene: repair and replication of DNA containing monoadducts and interstrand cross-links. *Cell* **50**, 789–799 (1987).
48. Derheimer, F. A., Hicks, J. K., Paulsen, M. T., Canman, C. E. & Ljungman, M. Psoralen-induced DNA interstrand cross-links block transcription and induce p53 in an ataxia-telangiectasia and Rad3-related-dependent manner. *Mol. Pharmacol.* **75**, 599–607 (2009).

Acknowledgements We thank D. Pellman and members of the Walter laboratory for comments on the manuscript, and K. Arnett for help with biolayer interferometry experiments. J.C.W. is supported by NIH grant HL098316 and a gift from the family of Jonathan G. Wiseman. R.A.W. is supported by American Cancer Society postdoctoral fellowship 131415-PF-17-168-01-DMC, D.R.S. by NIH award K99GM129422, D.R.S. and G.C. by Jane Coffin Childs postdoctoral fellowships, J.L.S. by a Damon Runyon postdoctoral fellowship, M.W. by the Cancer Research UK Clinician Scientist Fellowship, and E.L. by NIH award F31GM122277. J.C.W. is a Howard Hughes Medical Institute Investigator and an American Cancer Society Research Professor.

Reviewer information *Nature* thanks Daniel Durocher, Michael Seidman and the other anonymous reviewer(s) for their contribution to the peer review of this work.

Author contributions R.A.W. identified TRAIP as the E3 ligase that ubiquitylates CMG and characterized the role of TRAIP in cisplatin-ICL repair. D.R.S. characterized the role of CMG ubiquitylation in AP-ICL repair and performed the structure–function analysis of NEIL3. A.N.K.-L., M.R.H. and M.W. generated Fig. 4d and Extended Data Fig. 9 under the supervision of K.J.P. O.V.K. generated Fig. 1c, d and Extended Data Figs. 2i and 6a, b. G.C. and E.L. prepared *Xenopus laevis* rCMG. R.A. generated Fig. 1e and Extended Data Fig. 3c, d. J.L.S. generated Fig. 2e and Extended Data Fig. 4c. L.D. generated Extended Data Fig. 10b, c. C.A.M. helped to generate Extended Data Fig. 8b, d, e. J.C.W., R.A.W. and D.R.S. designed experiments, analysed the data and wrote the paper with input from the other authors.

Competing interests The authors declare no competing interests.

Additional information
Extended data is available for this paper at https://doi.org/10.1038/s41586-019-1002-0.
Supplementary information is available for this paper at https://doi.org/10.1038/s41586-019-1002-0.
Reprints and permissions information is available at http://www.nature.com/reprints.
Correspondence and requests for materials should be addressed to J.C.W.
Publisher's note: Springer Nature remains neutral with regard to jurisdictional claims in published maps and institutional affiliations.

METHODS

All experiments were performed at least twice, with a representative result shown. All oligonucleotide sequences are listed in Supplementary Table 1. No statistical methods were used to predetermine sample size. With the exception of Fig. 1e, the experiments were not randomized and the investigators were not blinded to allocation during experiments and outcome assessment.

Preparation of pICL. Preparations of the following plasmids containing site-specific crosslinks were performed as previously described: pICL$^{Pt;}$ (ref. [2]), pICL-*lacO*$^{Pt;}$ (ref. [7]), and pICL^{AP} and pICL-*lacO*$^{AP;}$ (ref. [1]). In brief, purified cisplatin- or AP-crosslinked oligonucleotide duplexes comprising Pt_Top and Pt_Bottom or AP_Top and AP_Bottom, respectively, were ligated into a parental plasmid linearized with BbsI, and the resulting supercoiled plasmid was isolated by caesium chloride gradient.

Preparation of pDPC$^{2\times lead}$. Preparation of pDPC$^{2\times lead}$ was performed as previously described[3,28]. In brief, oligonucleotide DPC_Fluoro_dC was ligated into a parental plasmid nicked with Nt.BbvCI and then crosslinked to recombinant *Haemophilus parainfluenzae* methyltransferase M.HpaII-His$_6$.

***Xenopus* egg extracts and DNA replication.** All animal work was approved by the Harvard Medical Area Standing Committee on Animals (HMA IACUC Study ID IS00000051-3, approved 25 October 2017). The institution has an approved Animal Welfare Assurance (A3431-01) from the Office of Laboratory Animal Welfare. *Xenopus laevis* female frogs (aged >2 years) were used as a source of eggs for the preparation of extracts, which were prepared essentially as described[29]. For DNA replication, plasmids were licensed by incubation in high-speed supernatant of egg cytoplasm at room temperature for 30 min at a final concentration of 7.5 ng pICL per μl extract (for replication intermediate and nascent strand analyses) or 15 ng pICL per μl extract (for plasmid pull-down and electron microscopy analyses) and, where indicated, 0.375 ng pQnt per μl extract. For reactions using pICL-*lacO* plasmids with a pre-assembled LacR array, the plasmid was incubated for 1 h at room temperature with purified biotinylated LacR[30] at a final concentration of 14 μM before licensing as described above. To inhibit licensing, Geminin was added to high-speed supernatant at a final concentration of 10 μM and incubated for 10 min at room temperature before the addition of DNA. Replication was initiated by addition of two volumes of nucleoplasmic egg extract (NPE). In all figures except Extended Data Fig. 10b, c, the addition of NPE corresponds to the 0 min time point. For nascent strand radiolabelling, reactions were supplemented with trace amounts of [α-^{32}P]dATP. Where indicated, reactions were supplemented with 200 μM NMS-873 p97 inhibitor (Sigma-Aldrich), 200 μM MLN4924 Cullin RING ligase inhibitor (Active Biochem), 111 μM RO-3306 CDK1 inhibitor (EMD Millipore), 100 μM ETP-46464 ATR inhibitor (Sigma-Aldrich), 50 μM PHA-767491 hydrochloride CDC7 inhibitor (Sigma-Aldrich), and/or 100 μM recombinant His$_6$-tagged ubiquitin (Boston Biochem) and incubated for 5 min before addition of the licensing reaction, unless otherwise indicated. To generate mitotic extract, NPE was supplemented with 50 ng μl^{-1} CDK1-Cyclin B1 (Life Technologies). Reactions were supplemented with approximately 30 to 50 nM recombinant NEIL3–Flag and 50 nM recombinant TRAIP, with the following exceptions: extracts used in Figs. 2f, 3c and Extended Data Fig. 5a were supplemented with 600 nM rTRAIP and those used in Extended Data Fig. 3a were supplemented with 20 nM rTRAIP.

Antibodies and immunodepletions. Rabbit polyclonal antibodies raised against the following *X. laevis* proteins have been previously described: BRCA1[31]; CDC45 and MCM7[32]; CLASPIN[33]; CUL2, LRR1 and TRAIP[23]; FANCM[28]; MCM6 and NEIL3[1]; MCM10[34]; DNA Pol ε (p60 subunit)[35]; and PCNA[36]. Rabbit polyclonal antibody against *X. laevis* DNA Pol ε subunit 3 was raised against the peptide MAERPEDLNLPNAVC by New England Peptide. Rabbit polyclonal antibody against *X. laevis* DNA Pol ε catalytic subunit was raised against the peptide MVLQNSGKFRAESRGDC by New England Peptide. Rabbit polyclonal Flag antibody raised against Flag peptide was prepared by New England Peptide. Rabbit polyclonal antibody raised against human FANCD2 has been previously described[37]. Rabbit polyclonal histone H3 antibody 9715 was purchased from Cell Signaling Technology. Mouse monoclonal histidine tag antibody AD1.1.10 was purchased from Bio-Rad. Rabbit polyclonal MCM3 antibody sc-292857 was purchased from Santa Cruz Biotechnology. Rabbit polyclonal MCM4 antibody A300-193A and MCM5 antibody A300-195A were purchased from Bethyl Laboratories. Rabbit polyclonal NEIL3 antibody 11621-1-AP was purchased from ProteinTech Europe. Rabbit polyclonal human phospho-CHK1 (Ser345) antibody 2341 was purchased from Cell Signaling Technology. Rabbit polyclonal antibody against *X. laevis* PSF1 was raised against the peptide LPRWKSEQLIRQGVLEHVLS by Bethyl Laboratories. Rabbit polyclonal antibody against *X. laevis* PSF3 was raised against the peptide ITASNLVQNYKKRKFNEADA by Bethyl Laboratories. Rabbit polyclonal TIMELESS antibody ab50943 was purchased from Abcam. Mouse monoclonal ubiquitin antibody sc-8017 was purchased from Santa Cruz Biotechnology. Mouse monoclonal vinculin V284 antibody 05-386 was purchased from EMD Millipore. The following antibodies were generous gifts: AND1 (A. Dutta, University of Virginia), CTF18 (T. Takahashi, Kyushu University), MCM2 (J. Mendez, Centro Nacional de Investigaciones Oncológicas) and TIPIN (V. Costanzo, FIRC Institute for Molecular Oncology). Immunodepletions of BRCA1[21] and LRR1[23] were performed as previously described except in Extended Data Fig. 3l–n, for which BRCA1 serum was first purified on Protein A Sepharose before use in depletion. For TRAIP depletions, 2.5 volumes of 1 mg ml^{-1} Protein A Sepharose-purified antibodies against TRAIP were gently rotated with 1 volume of Protein A Sepharose beads overnight at 4 °C. Five volumes of egg extract were depleted by three rounds of gentle rotation with one volume of antibody-bound beads for 1 h at 4 °C. For NEIL3 depletions, 2.5 volumes of 1 mg ml^{-1} Protein A Sepharose-purified antibodies against NEIL3 were gently rotated with 1 volume of Protein A Sepharose beads overnight at 4 °C. Five volumes of egg extract were depleted by three rounds of gentle rotation with one volume of antibody-bound beads for 20 min at room temperature. For FANCM depletions, 4 volumes of 1 mg ml^{-1} affinity-purified antibodies against FANCM were gently rotated with 1 volume of Protein A Sepharose beads overnight at 4 °C. Five volumes of egg extract were depleted by three rounds of gentle rotation with one volume of antibody-bound beads for 1 h at 4 °C. For FANCD2 and NEIL3 double depletion, 3 volumes of 1 mg ml^{-1} affinity-purified antibodies against NEIL3 were gently rotated with 1 volume of Protein A Sepharose beads for 2 h at 4 °C. Three volumes FANCD2 anti-serum were then added to the Protein A Sepharose beads and incubation was continued at 4 °C overnight. Five volumes of egg extract were depleted by three rounds of gentle rotation with 1 volume of antibody-bound beads for 20 min at room temperature.

Replication intermediate analysis. Replication reactions were stopped at the indicated time points with 10 volumes of Stop Solution A (5% SDS, 80 mM Tris-HCl (pH 8.0), 0.13% phosphoric acid, 10% Ficoll, and 0.5% bromophenol blue). The reactions were treated with 4 mg ml^{-1} Proteinase K (Roche) for 1 h at 37 °C and resolved by 0.8% native agarose gel electrophoresis. The gels were then dried and visualized by phosphorimaging on a Typhoon FLA 7000 (GE Healthcare). Image contrast was occasionally adjusted to improve visualization of bands.

Nascent strand analysis. Replication reactions were stopped at the indicated time points with 10 volumes of Stop Solution B (0.5% SDS, 50 mM Tris-HCl (pH 7.5) and 25 mM EDTA (pH 8.0)). The reactions were treated with 0.16 mg ml^{-1} RNase A for 1 h at 37 °C, followed by 0.75 mg ml^{-1} Proteinase K overnight at room temperature. The reactions were then phenol/chloroform extracted, precipitated, and digested with AflIII (for pICL^{Pt}) for 3 h at 37 °C or Nb.BsmI (for pDPC$^{2\times lead}$) for 1 h at 65 °C. After addition of denaturing PAGE Gel Loading Buffer II (Life Technologies), the radiolabelled nascent strands were resolved on a 7% denaturing polyacrylamide gel, transferred to filter paper, dried, and visualized by phosphorimaging on a Typhoon FLA 7000 (GE Healthcare). To enhance the visualization of bands, a logarithmic transform was applied using ImageJ to all nascent strand analyses except those presented in Fig. 2e and Extended Data Figs. 3a, e and 7e. Sequencing gel markers were generating using the Thermo Sequenase Cycle Sequencing Kit (USB Corporation) with primer pICL_Seq that anneals with the pICL plasmids 149 nucleotides upstream of the crosslink.

Plasmid pull-down. Plasmid pull-downs were performed essentially as described[38]. In brief, streptavidin-coupled magnetic beads (Invitrogen) were gently rotated with biotinylated LacR[30] for 40 min at room temperature. The beads were washed three times with 20 mM HEPES-KOH (pH 7.7), 100 mM KCl, 5 mM $MgCl_2$, 250 mM sucrose, 0.25 mg ml^{-1} BSA and 0.02% Tween-20, then resuspended in the same buffer. Replication reactions were mixed with the beads at the indicated times and gently rotated for 30 min at 4 °C. The beads were washed three times with 20 mM HEPES-KOH (pH 7.7), 100 mM KCl, 5 mM $MgCl_2$, 0.25 mg ml^{-1} BSA, and 0.03% Tween-20, then resuspended in 2x Laemmli buffer for analysis by immunoblotting.

Ubiquitin linkage analysis. A plasmid for expression of the AMSH* deubiquitylating enzyme (pOINB-AMSH*)[39] was obtained from AddGene (Plasmid 66712). AMSH* expression was induced in 1 l Rosetta 2 (DE3) pLysS cells (Novagen) with 0.4 mM IPTG for 18 h at 18 °C. Bacterial cell pellets were suspended in binding buffer (20 mM Tris-HCl (pH 8.5), 300 mM NaCl, 50 mM imidazole, 2 mM β-mercaptoethanol and 1x Roche cOmplete protease inhibitor cocktail) and sonicated. The soluble lysate was collected after centrifugation at 25,000 r.p.m. in a SW40.1 rotor for 1 h and bound to TALON resin (Clonetech) for 90 min at 4 °C. The bound resin was then washed with 1 l binding buffer and AMSH* was eluted with binding buffer containing 250 mM imidazole. The eluate was then concentrated and dialysed against 20 mM Tris-HCl (pH 8.5), 150 mM NaCl and 4 mM dithiothreitol (DTT) at 4 °C and 6 μM aliquots were stored at −80 °C. Analysis of ubiquitin chains on MCM7 and MCM4 was performed using UbiCrest deubiquitylating enzymes (Boston Biochem). Plasmid pull-downs were performed as described above, except that the beads were resuspended in 1x DUB reaction buffer (50 mM Tris-HCl (pH 7.5), 50 mM NaCl, 5 mM DTT) and then incubated with 5 μM USP2$_{CD}$, 8 μM Otubain1 (OTUB1), 0.6 μM AMSH*, 1x Yod1, 1x OTUD3, 1x Trabid, 1x Cezanne or 1x Otulin for 30 min at 37 °C. Reactions were quenched with an equal volume of 2x Laemmli buffer and analysed by immunoblotting.

Immunoblotting. Samples were resolved on Mini-PROTEAN or Criterion TGX precast gels (Bio-Rad) and transferred to PVDF membranes (Perkin Elmer). Membranes were blocked in 5% non-fat milk in 1x PBST for 60 min at room temperature, then incubated with antibody diluted in 1x PBST containing 1% BSA overnight at 4 °C. After extensive washing in 1x PBST at room temperature, the membranes were incubated with goat anti-rabbit horseradish peroxidase-conjugated antibodies (Jackson ImmunoResearch) diluted in 5% non-fat milk in 1x PBST for 1 h at room temperature. Membranes were washed extensively in 1x PBST, briefly incubated with HyGLO chemiluminescent HRP antibody detection reagent (Denville), and imaged using an Amersham Imager 600 (GE Healthcare). Contrast was occasionally adjusted to improve visualization of bands.

Error-free repair assay. The error-free repair assay was performed as previously described[40]. In brief, replication reactions were stopped at the indicated time points with 10 volumes of Stop Solution B. The reactions were treated with 0.16 mg ml^{-1} RNase A for 1 h at 37 °C, followed by 0.75 mg ml^{-1} Proteinase K overnight at room temperature. The reactions were then phenol/chloroform extracted, precipitated and digested with HincII or HincII and SapI for 3 h at 37 °C. After the addition of 0.17 volumes of DNA loading buffer (10 mM Tris-HCl (pH 7.5), 60% glycerol and 0.5% bromophenol blue), the digestion products were resolved by 0.8% native agarose gel electrophoresis, dried, and visualized by phosphorimaging on a Typhoon FLA 7000 (GE Healthcare). Repair products were quantified using ImageJ (NIH).

Purification of recombinant *Xenopus* NEIL3. *X. laevis* NEIL3 was purified as previously described[1]. In brief, constructs for the expression of rNEIL3-NZF(C/A), rNEIL3(T310L/L311V), rNEIL3(K500E), rNEIL3(K546E), rNEIL3(K500E/K546E) and rNEIL3(Δ92) were prepared by digesting Integrated DNA Technologies gene blocks encompassing the C-terminal domain of NEIL3 (with Flag epitope tag) and containing the indicated mutations with BbvCI and XhoI and then ligating the fragments into similarly digested pFastBac1-NEIL3–Flag[1]. The rNEIL3(Δ291) expression construct was prepared by PCR amplification of the NEIL3 glycosylase domain from a *X. laevis* cDNA library (a gift from T. G. W. Graham) using primers NEIL3_291_A and NEIL3_291_B. The fragment was then digested with EcoRI and XhoI and ligated into similarly digested pFastBac1 (Thermo Fisher Scientific). All mutations and truncations were confirmed by Sanger sequencing. Baculoviruses expressing rNEIL3 were then prepared using the Bac-to-Bac system (Thermo Fisher Scientific) according to the manufacturer's protocols. rNEIL3 protein was expressed in 250 ml suspension cultures of Sf9 insect cells (Expression Systems) by infection with baculovirus expressing NEIL3–Flag for 48–72 h. Sf9 cells were collected and suspended in 10 ml NEIL3 Lysis Buffer (50 mM Tris-HCl (pH 7.5), 300 mM NaCl, 10% glycerol, 1x Roche EDTA-free cOmplete protease inhibitor cocktail, 0.5 mM PMSF and 0.2% Triton X-100). Cells were lysed by sonication, and the soluble fraction was collected by spinning the lysate at 25,000 r.p.m. in a Beckman SW41 rotor for 1 h. The soluble lysate was incubated with 200 μl anti-Flag M2 affinity resin (Sigma-Aldrich) for 90 min at 4 °C. The resin was washed once with 10 ml Lysis Buffer, twice with NEIL3 Wash Buffer (50 mM Tris-HCl (pH 7.5), 300 mM NaCl, 10% glycerol and 0.2% Triton X-100), and three times with Buffer A (50 mM Tris-HCl (pH 7.5), 300 mM NaCl and 10% glycerol). NEIL3–Flag protein was eluted from the resin with Buffer A containing 100 μg ml^{-1} 3×Flag peptide (Sigma-Aldrich). Elution fractions containing NEIL3–Flag protein were pooled and dialysed against 50 mM HEPES-KOH (pH 7.0), 300 mM NaCl, 1 mM DTT and 20% glycerol at 4 °C for 12 h and then dialysed against 50 mM HEPES-KOH (pH 7.0), 150 mM NaCl, 1 mM DTT and 15% glycerol at 4 °C for 3 h. Aliquots of protein were stored at −80 °C. Constructs for expression of GST-TEV-NZF (GST, glutathione *S*-transferase; TEV, tobacco etch virus) fusion proteins were prepared by PCR amplification of the NEIL3 NZF from pFastBac1-NEIL3–Flag and pFastBac1-NEIL3(T310L/L311V)–Flag using primers NEIL3_NZF_A and NEIL3_NZF_B. The pGEX-6P-1 backbone (with GST-TEV tag) was PCR-amplified from pGEX-6P-1-GST-TEV–Flag-UBXN7 with primers GST_A and GST_B. The resulting fragments were then assembled using the NEBuilder HiFi DNA assembly cloning kit (New England Biolabs) according to the manufacturer's instructions. Expression of GST-TEV-NZF proteins was induced in 1 l Rosetta 2 (DE3) pLysS cells (Novagen) with 0.5 mM IPTG for 3 h at 37 °C. Bacterial cell pellets were suspended in Buffer A (10 mM sodium phosphate (pH 7.4), 150 mM NaCl, 5 mM β-mercaptoethanol, 10 μM $ZnCl_2$ and 1x Roche cOmplete protease inhibitor cocktail) and sonicated. The soluble lysate was collected after centrifugation at 25,000 r.p.m. in a SW40.1 rotor for 1 h and bound to Glutathione Sepharose 4B (GE Healthcare) for 1.5 h at 4 °C. The bound resin was then washed five times with Buffer A and protein was eluted with Buffer B (50 mM Tris-HCl (pH 8.0), 150 mM NaCl, 10 μM $ZnCl_2$, 5 mM β-mercaptoethanol and 20 mM glutathione). Fractions containing GST-TEV-NZF fusion proteins were dialysed against 50 mM Tris-HCl (pH 8.0), 150 mM NaCl, 10 μM $ZnCl_2$, 5 mM β-mercaptoethanol and 10% glycerol at 4 °C and aliquots were stored at −80 °C. Constructs for expression of MBP-TEV-GRF ZF fusion proteins were prepared by amplifying the NEIL3 GRF ZF1 or GRF ZF2 from pFastBac1-NEIL3–Flag or pFastBac1-NEIL3(K500E/K546E)–Flag using primers GRFZF1_A and GRFZF1_B or GRFZF2_A and GRFZF2_B, respectively. The MBP tag was PCR-amplified using the primers MBP_A and MBP_B or MBP_A and MBP_C for GRF ZF1 and GRF ZF2 respectively. The pGEX-6P-1 backbone was PCR-amplified from pGEX-6P-1-GST-TEV–Flag-UBXN7 with primers pGEX_A and pGEX_B. The resulting fragments were then assembled using the NEBuilder HiFi DNA assembly cloning kit (New England Biolabs) according to the manufacturer's instructions. Expression of MBP-TEV-GRF ZF proteins was induced in 1 l Rosetta 2 (DE3) pLysS cells (Novagen) with 0.5 mM IPTG for 3 h at 37 °C. Bacterial cell pellets were suspended in Buffer C (20 mM Tris-HCl (pH 7.5), 300 mM NaCl, 1 mM DTT and 1x Roche cOmplete protease inhibitor cocktail) and sonicated. The soluble lysate was collected after centrifugation at 25,000 r.p.m. in a SW40.1 rotor for 1 h and bound to amylose resin (New England Biolabs) for 1.5 h at 4 °C. The bound resin was then washed six times with Buffer C and protein was eluted with Buffer C containing 10 mM maltose. Fractions containing MBP-TEV-GRF ZF fusion proteins were dialysed against 20 mM Tris-HCl (pH 8.0), 200 mM NaCl, 1 mM DTT and 10% glycerol at 4 °C and aliquots were stored at −80 °C.

Purification of recombinant *Xenopus* TRAIP. The *X. laevis* TRAIP open reading frame was PCR-amplified from a *X. laevis* cDNA library (a gift from T. G. W. Graham) using primers TRAIP_A and TRAIP_B or TRAIP_C and TRAIP_D. For expression in bacteria, the product amplified with TRAIP_A and TRAIP_B was gel-isolated, digested with BamHI and ligated into pH_6-SUMO[41] linearized with BamHI. For expression in Sf9 insect cells, the product amplified with TRAIP_C and TRAIP_D was gel-isolated, digested with BssHII and NotI, and ligated in pFastBac1 (Life Technologies) digested with BssHII and NotI. A 3×Flag tag and 3C protease cleavage site were introduced by linearizing the resulting plasmid with BssHII and ligating a linker comprising annealed oligonucleotides 3×F_3C_Top_1, _2, _3 and 3×F_3C_Bottom_1, _2, _3, and _4. The R18C substitution was introduced by 'around-the-horn' PCR[42] using primers R18C_A and R18C_B. pH_6-SUMO-TRAIP(ΔPIP) (residues 1–455) was constructed by around-the-horn PCR using primers PIP_A and PIP_B. All mutations and truncations were confirmed by Sanger sequencing.

His_6-SUMO-TRAIP was expressed in Rosetta 2 (DE3) pLysS (Novagen) by induction with 0.1 mM IPTG overnight at 16 °C in growth media supplemented with 50 μM $ZnSO_4$. Bacterial pellets were resuspended in TRAIP Lysis Buffer (20 mM HEPES-NaOH (pH 7.5), 400 mM sodium acetate, 10% glycerol, 10 μM $ZnSO_4$, 0.1% NP-40, 1 mM DTT and 1x Roche cOmplete protease inhibitor cocktail) supplemented with 20 mM imidazole. After sonication, ammonium sulfate and polyethyleneimine were added to the lysate to final concentrations of 300 mM and 0.45%, respectively and incubated for 15 min at 4 °C. The soluble fraction was collected after centrifugation at 40,000*g* for 45 min at 4 °C, and precipitated with saturating ammonium sulfate. The precipitated fraction was collected after centrifugation at 40,000*g* for 45 min at 4 °C, resuspended in Lysis Buffer, and then rotated with NiNTA resin (Qiagen) for 30 min at room temperature. The resin was washed three times with Wash Buffer (20 mM HEPES-NaOH (pH 7.5), 400 mM sodium acetate, 10% glycerol, 20 mM imidazole, 10 μM $ZnSO_4$, 0.01% NP-40, 1 mM DTT and 1x Roche cOmplete protease inhibitor cocktail). His_6-SUMO-TRAIP was eluted from the resin with Elution Buffer (20 mM HEPES-NaOH (pH 7.5), 400 mM sodium acetate, 10% glycerol, 250 mM imidazole, 0.01% NP-40 and 1 mM DTT). Elution fractions containing His_6-SUMO-TRAIP were pooled and dialysed against Dialysis Buffer (20 mM HEPES-NaOH (pH 7.5), 400 mM sodium acetate, 10% glycerol, 0.01% NP-40 and 1 mM DTT) supplemented with 120 mM imidazole overnight at 4 °C. With the exception of the indicated proteins used in Extended Data Figs. 2b, g, h, and 6e, the His_6-SUMO was simultaneously cleaved by the addition of 0.03 mg ml^{-1} Ulp1 during dialysis. Aliquots were flash frozen and stored at −80 °C.

Baculoviruses expressing 3×Flag-3C-rTRAIP (wild-type) or 3×Flag-3C-rTRAIP(R18C) were prepared using the Bac-to-Bac system (Thermo Fisher Scientific) according to the manufacturer's protocols. rTRAIP protein was expressed in 200 ml suspension cultures of Sf9 insect cells (Life Technologies) by infection with baculovirus for 72 h. Sf9 cells were collected and suspended in 10 ml TRAIP Lysis Buffer. After sonication, the soluble lysate was collected after centrifugation at 30,000 r.p.m. in a 45Ti rotor for 1 h and bound to anti-Flag M2 affinity agarose gel (Sigma-Aldrich) for 2 h at 4 °C. The bound resin was then washed five times with TRAIP Lysis Buffer and eluted with TRAIP Lysis Buffer supplemented with 100 μg ml^{-1} 3× Flag peptide (Sigma-Aldrich). Elution fractions containing 3×F-3C-rTRAIP were pooled incubated overnight at 4 °C in the presence of 3C protease. Aliquots were flash-frozen and stored at −80 °C.

Purification of recombinant *Xenopus* CMG. The open reading frames encoding the eleven *X. laevis* CMG subunits (CDC45, MCM2-7 hetero-hexamer, and GINS hetero-tetramer) were cloned into a single plasmid (pGC187) using the MultiBac system[43]. MCM2-7 open reading frames were PCR-amplified from *X. laevis* cDNA. A sequence encoding the Flag tag was added to the N terminus of MCM3. Codon-optimized GINS and CDC45 open reading frames were synthesized as gBlocks by IDT. The bacmid encoding the CMG complex was obtained by electroporating

pGC187 into DH10EMBacY (Geneva Biotech) electro-competent cells and purified using ZR BAC DNA miniprep kit (Zymo Research).

CMG baculovirus was generated by transfecting pGC187 bacmid into Sf9 cells (Expression Systems) for 96 h, and amplifying the virus in two rounds of 96 h each. Individual subunit expression levels were monitored by immunoblotting. 500 ml of Tni (similar to HiFive) cell culture (Expression Systems) at a density of 2–3 million cells per ml was infected with 50 ml baculovirus (multiplicity of infection > 10). Cells collected 72 h post-infection were pelleted at 500*g* for 15 min, frozen in liquid nitrogen and stored at −80 °C.

The frozen pellet was re-suspended to a final volume of 50 ml in CMG Lysis Buffer (CLB; 20 mM Tris-HCl (pH 7.5), 10% glycerol, 5 mM magnesium acetate, 300 mM potassium acetate, 0.1% Tween20, 1 mM PMSF, 0.2 mM ATP and 1x Roche EDTA-free cOmplete protease inhibitor cocktail). Cells were lysed by sonication on ice or by Dounce homogenization and the insoluble fraction was pelleted via centrifugation for 1 h at 30,000*g* at 4 °C. The clarified lysate was incubated with 1 ml M2 anti-Flag resin (Sigma-Aldrich) for 1 h at 4 °C on a rotating wheel. The resin was washed five times with 10 ml of CLB in a disposable column. The protein was eluted twice with 1 ml each of CLB supplemented with 0.2 mg ml^{-1} 3×Flag peptide (Sigma-Aldrich) for 1 h at 4 °C. Eluted fractions were frozen in liquid nitrogen and stored at −80 °C until the ion-exchange polishing could be performed.

The ion exchange polishing procedure was adapted from a previous study[44]. Ion exchange was performed on a GE AKTA FPLC using CMG Start Buffer (25 mM HEPES (pH 7.6), 10% glycerol, 0.02% Tween20, 1 mM EDTA, 1 mM EGTA, 0 mM KCl, 0.4 mM PMSF, 1 mM DTT) and CMG Elution Buffer (25 mM HEPES (pH 7.6), 10% glycerol, 0.02% Tween20, 1 mM EDTA, 1 mM EGTA, 1,000 mM KCl, 0.4 mM PMSF and 1 mM DTT). The Flag eluate was diluted threefold with CMG Start Buffer to a final salt concentration of 100 mM and loaded onto two columns connected in tandem: MonoS 5/50 GL (GE Healthcare) and MonoQ 5/50 GL (GE Healthcare) such that the flowthrough from MonoS passed through MonoQ. In this scheme, MonoS trapped some contaminants whereas MonoQ bound CMG and its subcomplexes. After loading the protein, the columns were washed with 10 ml of 10% CMG Elution Buffer, then MonoS was disconnected. MonoQ was eluted with 30 ml 10–60% CMG Elution Buffer gradient and 0.5 ml fractions were collected. Stoichiometric CMG complex eluted at 450–500 mM KCl. CMG stoichiometry and purity were verified by SDS–PAGE imaged with SYPRO Ruby. A preparation from 0.5 l of Tni cell culture usually yielded 0.1 mg of very pure CMG (Extended Data Fig. 5d).

Purified CMG was further concentrated by ion exchange on a MonoQ PC 1.6/5 (GE Healthcare) using an AKTA FPLC as previously described[44], or by ion exchange on small volumes of NuviaQ resin (Bio-Rad). To perform the latter, MonoQ fractions containing CMG were diluted threefold with CMG Start Buffer for a final KCl concentration of 150 mM and incubated for 1 h at 4 °C with 40 μl of NuviaQ resin pre-equilibrated in 15% CMG Elution Buffer. The resin was washed three times with 400 μl 15% CMG Elution Buffer in a small disposable column (Pierce), then three times with 400 μl 30% CMG Elution Buffer. Each time the flowthrough was collected via centrifugation for 30 s at 500*g* in a refrigerated tabletop centrifuge with a swing-bucket rotor. CMG was eluted by incubating the washed resin with 40 μl 60% CMG Elution Buffer for 15 min and collected via centrifugation. Any protein that remained bound to the resin was eluted with 40 μl 100% CMG Elution Buffer. Aliquots (3–5 μl) of concentrated CMG (0.5–1.0 μM) were frozen in liquid nitrogen and stored at −80 °C.

In vitro CMG ubiquitylation assay. A ubiquitylation assay using an equimolar mixture of the E2 ubiquitin conjugating enzymes UbcH5a, UbcH5b, and UbcH5c, wild-type rTRAIP or rTRAIP(R18C) at an approximate final concentration of 15 nM, and, where included, recombinant CMG at an approximate final concentration of 150 nM was performed using the Enzo BML-UW9920 Ubiquitinylation Kit according to the manufacturer's instructions (Enzo Life Sciences). Reaction products were then resuspended in 1x Laemmli buffer and analysed by immunoblotting. For reactions containing rCMG, products were bound to anti-Flag M2 affinity agarose gel (Sigma-Aldrich) for 30 min at room temperature. Bound beads were washed 3 times with egg lysis buffer (10 mM HEPES (pH 7.7), 50 mM KCl, 2.5 mM $MgCl_2$, 2.5 M sucrose), and treated with USP2 for 30 min at 37 °C as indicated before immunoblotting.

Electron microscopy. Electron microscopy analysis of the replication intermediates was performed as previously described[9]. In brief, replication reactions were stopped at 90 min with 10 volumes of Stop Solution C (100 mM Tris-HCl (pH 7.5), 6.7 mM $MgCl_2$, 1 mM EDTA (pH 8.0) and 1% SDS). The DNA was crosslinked with trimethylpsoralen (Sigma-Aldrich) and irradiation with UV light at 365 nM before protein extraction and DNA purification. Purified DNA was incubated with *Escherichia coli* single-stranded DNA binding protein, fixed with 0.3% glutaraldehyde, then purified by size-exclusion chromatography. Eluted complexes were mounted onto grids, which were then subjected to rotary shadowing with platinum and carbon coating using a Leica Ace600 coating system. Samples were imaged using a JEOL 1200EX transmission electron microscope equipped with a 2k charge-coupled device camera (Advanced Microscopy Techniques). After blinding the scorer to the conditions, reversed forks were counted and expressed as a percentage of pre-incision structures, which was then normalized to the mock-depleted condition.

Electrophoretic mobility shift assay. MBP-TEV-GRF ZF fusion protein was incubated with 10 nM 5′-end-radiolabelled 25mer ssDNA (EMSA_Top) or double-stranded (ds)DNA (EMSA_Top + EMSA_Bottom) in buffer containing 1 mM $MgCl_2$, 100 μM $ZnSO_4$, 10 mM Tris-HCl (pH 8.0), 50 mM NaCl, 0.2 mM TCEP and 5% glycerol for 30 to 60 min at 4 °C. Binding reactions were separated on native 5% acrylamide (37.5:1), 45 mM Tris, 45 mM borate, 1 mM $MgCl_2$, 100 μM $ZnSO_4$ gels and visualized by phosphorimaging on a Typhoon FLA 7000 (GE Healthcare).

NEIL3 glycosylase assay. AP-ICLs between complementary DNA and DNA/RNA chimaeric oligonucleotides AP_assay_A and AP_assay_B were crosslinked, RNase H digested, and gel purified as described[1]. To monitor the unhooking of AP-ICLs, 2.5 nM 5′-radiolabelled crosslinked substrate was incubated with 20 nM rNEIL3–Flag in 20 mM HEPES-KOH (pH 7.0), 50 mM NaCl, 1 mM DTT and 0.1 mg ml^{-1} BSA at 37 °C[45]. Reactions were quenched with 1 volume of 2x formamide buffer (86% formamide, 2x TBE, 20 mM EDTA (pH 8.0)), separated on a denaturing polyacrylamide and visualized by phosphorimaging on a Typhoon FLA 7000 (GE Healthcare).

Biolayer interferometry. All measurements were obtained using an OctetRED384 instrument (Pall ForteBio) in the Center for Molecular Interactions at Harvard Medical School. Samples in 0.2 ml BLI buffer (1x PBS, 0.1 mg ml^{-1} BSA and 0.05% Tween 20) were dispensed into polypropylene 96-well black flat-bottom plates (Greiner Bio-One). GST-TEV-NZF or GST control protein (30 μg ml^{-1}) was captured on pre-wet anti-GST biosensors (Pall ForteBio). Biosensors were then transferred to wells containing BLI buffer to enable dissociation of non-specifically bound GST-TEV-NZF protein and establish a measurement baseline. Biosensors were next transferred to wells containing serial dilutions of monoubiquitin (Boston Biochem) to monitor the association of ubiquitin with the immobilized GST-TEV-NZF protein. Finally, biosensors were transferred to wells containing BLI buffer to monitor the dissociation of ubiquitin from GST-TEV-NZF protein. For each ubiquitin concentration, the steady state ubiquitin binding response (R_{eq}) was determined from a five-second window at the end of the association phase. R_{eq} values were subsequently corrected for non-specific binding of ubiquitin to the GST epitope by subtracting R_{eq} values obtained for the GST control protein. Steady-state responses were plotted as a function of ubiquitin concentration ([Ub]) and the dissociation constant K_d was determined using the Prism software suite by fitting the data to the nonlinear regression equation $R_{eq} = \frac{R_{max} \times [Ub]}{[Ub] + K_d}$ where R_{max} is the globally constrained maximum association response.

Cell lines. Wild-type and *NEIL3*-knockout HAP1 near-haploid human cells were purchased as authenticated from Horizon Discovery and cultured at 37 °C and 5% CO_2 in IMDM (Gibco) supplemented with 10% fetal calf serum (Gibco) and penicillin/streptomycin (Gibco). *NEIL3*-knockout cells were confirmed by immunoblotting against NEIL3. For targeting of *FANCL*, wild-type and *NEIL3*-knockout cells were transfected with Turbofectin 8.0 (Origene) and the following plasmids: pX461, FANCL_left and FANCL_right CRISPR guides in U6 BsaI backbone, and *FANCL*-Puro targeting construct (Extended Data Fig. 9b). *FANCL* plasmids were obtained from the Wellcome Trust Sanger Institute. Two days post-transfection, 3.5 μg ml^{-1} puromycin (Gibco) was added, and two days later, cells were plated in 96-well plates with puromycin. After 14 days of incubation, individual clones were picked and analysed for *FANCL* targeting using the SequalPrep Long PCR kit (Applied Biosystems) (see Supplementary Table 1 for primer sequences). Targeted clones were then plated with 100 ng ml^{-1} mitomycin C (Sigma-Aldrich) overnight and analysed by immunoblotting for FANCD2. *FANCL* knockouts were identified by failure to ubiquitylate FANCD2 upon exposure to mitomycin C.

CH12-F3 murine B lymphoma cells (a generous gift from M. Neuberger, MRC Laboratory of Molecular Biology) were cultured at 37 °C and 5% CO_2 in RPMI (Gibco) supplemented with 10% fetal calf serum, penicillin/streptomycin, and 10 μM β-mercaptoethanol. To target *Neil3* and *Fancb*, CH12 cells were transfected using the Lonza Nucleofection Kit V and the following plasmids: pX458 and CRISPR guides against either *Neil3* exon 1 or 2 (Neil3_exon1 and Neil3_exon2) and/or a *Fancb* guide against exon 5 (Fancb_319). Two days after transfection, GFP-positive cells were singly sorted by flow cytometry into 96-well plates, and cultured for 7–10 days to obtain single colonies that were screened by PCR fragment analysis. The target exons of *Neil3* in putative clones were then amplified and cloned into the pMiniT 2.0 vector (NEB) and sequenced. *Neil3* clone 1 carried deletion in each allele of exon 2 of sizes 14- and 26-bp respectively, while clone 2 carried a 38- and 6-bp deletion in each allele of exon 1. *Fancb* clone 1 carried a 359-bp deletion in exon 5 and clone 2 carried a 21-bp deletion. *Neil3* clones were subsequently targeted for *Fancb* to generate double knockouts; clone 1 had a 4-bp deletion in *Fancb* exon 5, clone 2 had a 10-bp deletion, and clone 3 had a

24-bp deletion. Disruption of *Fancb* function was tested by treating all clones with mitomycin C before detection for the loss of FANCD2 monoubiquitylation by immunoblotting as described above.

All cell lines were tested to be mycoplasma negative using the MycoAlert Mycoplasma Detection Kit (Lonza).

Colony survival assay. For the cisplatin colony survival assay, HAP1 cells were prepared at 2×10^5 cells per ml. Cells and cisplatin (diluted in culture media) were mixed in 96-well blocks (Greiner Bio-One Masterblock) and foil seals (Bio-Rad Microseal 'F') were applied before culturing cells at 37 °C for 2 h. Cells were then serially diluted in PBS using a multi-channel pipette to obtain 1:10 and 1:100 dilutions, and 100 μl of each of three concentrations were plated in duplicate in 24-well plates filled with 1.5 ml of culture media per well. Cells were cultured for 6 days before being stained with crystal violet[46] and colonies were quantified by a GelCount colony counter (Oxford Optronix).

For the trioxsalen colony survival assay, cells were seeded in 24-well plates at 1.2×10^5 cells per well for 5 h before the addition of trioxsalen (Sigma-Aldrich) and then cultured for 1 h. Cells were then exposed to 6 kJ m^{-2} of UVA light (365 nm, VL-6.L lamp) through the bottom of the tissue culture plate to photoactivate trioxsalen. The cells were washed twice with culture media, incubated at 37 °C for 10 min to offload unbound trioxsalen, then washed again and treated with 12 kJ min^{-1} m^{-2} UVA to convert trioxsalen monoadducts into ICLs[47,48]. Cells were then trypsinized, diluted, plated, cultured, and stained as above.

Cell viability assay. CH12 cells were plated in flat-bottom 96-well plates at 5,000 cells per well and cultured with trioxsalen for 1 h, then exposed to 12 kJ min^{-1} m^{-2} UVA. Cells were then cultured for 3 days before being assayed with the CellTiter 96 AQueous One Solution Cell Proliferation Assay (Promega).

Reporting summary. Further information on research design is available in the Nature Research Reporting Summary linked to this paper.

Data availability

All relevant data are available from the authors and/or are included with this Letter. Source images are available in Supplementary Fig. 1.

49. Walter, J., Sun, L. & Newport, J. Regulated chromosomal DNA replication in the absence of a nucleus. *Mol. Cell* **1**, 519–529 (1998).
50. Klein Douwel, D. et al. XPF-ERCC1 acts in unhooking DNA interstrand crosslinks in cooperation with FANCD2 and FANCP/SLX4. *Mol. Cell* **54**, 460–471 (2014).
51. Long, D. T., Räschle, M., Joukov, V. & Walter, J. C. Mechanism of RAD51-dependent DNA interstrand cross-link repair. *Science* **333**, 84–87 (2011).
52. Fu, Y. V. et al. Selective bypass of a lagging strand roadblock by the eukaryotic replicative DNA helicase. *Cell* **146**, 931–941 (2011).
53. Sonneville, R. et al. CUL-2^{LRR-1} and UBXN-3 drive replisome disassembly during DNA replication termination and mitosis. *Nat. Cell Biol.* **19**, 468–479 (2017).

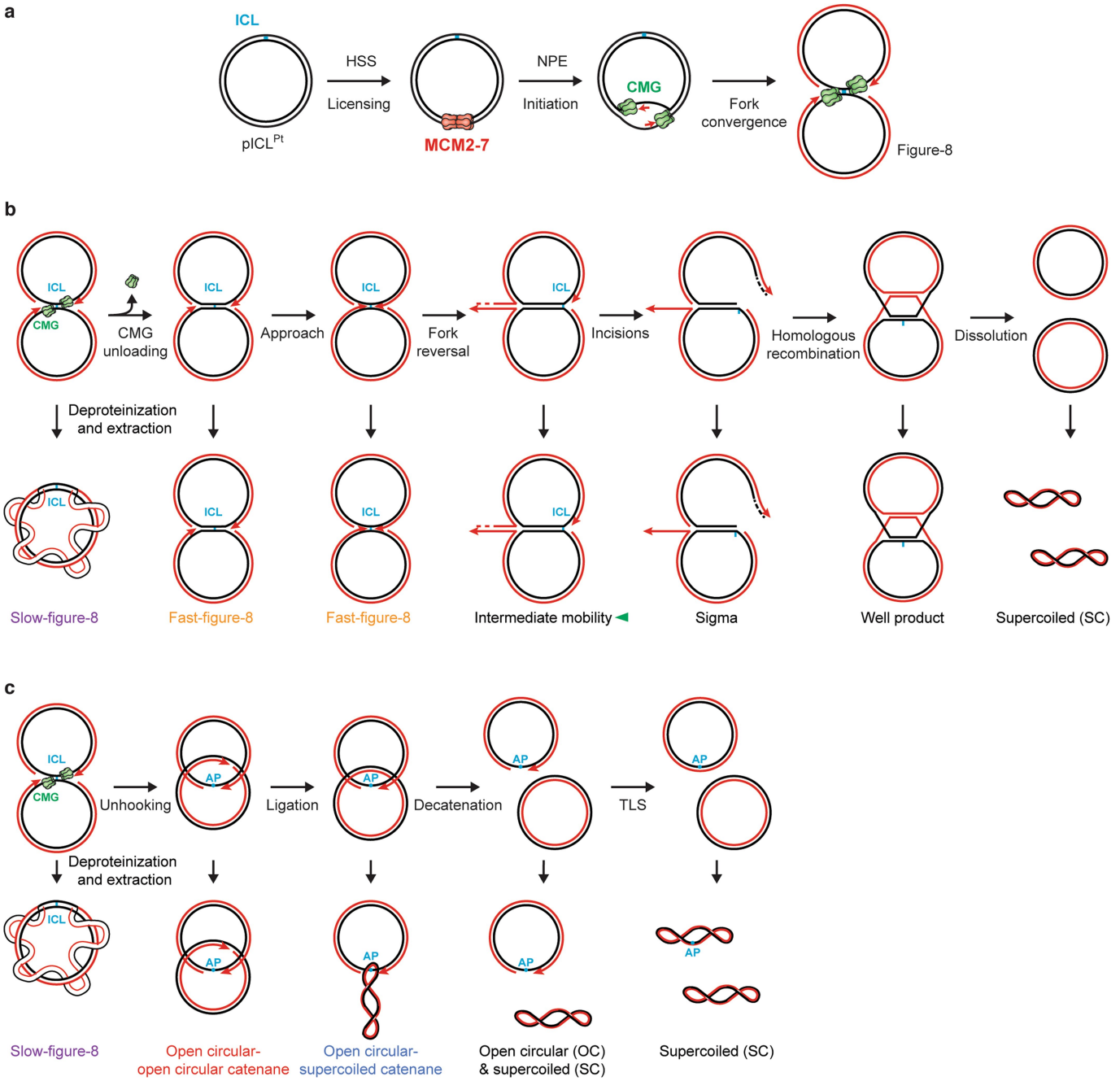

Extended Data Fig. 1 | DNA replication and ICL repair in *Xenopus* egg extracts. a, Schematic of pICL replication in the nucleus-free *Xenopus* egg extract system[49]. Incubation of the plasmid in high-speed supernatant supports the recruitment of inactive MCM2–MCM7 double hexamers (red hexamers; 'Licensing'). Addition of NPE activates replication initiation, including the assembly of active CMG helicases (green hexamers), and elongation of nascent strands (red lines) leads to convergence of forks at the ICL. **b**, Intermediates generated during replication-coupled repair of a cisplatin-ICL. Top, progression through the incision-dependent Fanconi anaemia repair pathway generates distinct intermediates resulting from fork convergence, CMG unloading, leading strand approach to the ICL, fork reversal, incisions, and repair of the double strand break by homologous recombination. Bottom, deproteinization of the DNA intermediates depicted along the top yields DNA structures that travel with characteristic mobilities during native agarose gel electrophoresis. These structures are indicated along the side of the gel and with coloured dots and/or arrows in Fig. 1b and other figures. The slow-figure-8 species arise upon fork convergence on the ICL (Fig. 1b, purple dot). Conversion of slow- to fast-figure-8 species results from CMG unloading and an accompanying change in plasmid topology[9] (Fig. 1b, orange dot). Next, a species of intermediate mobility appears (Fig. 1b, green arrow), which represents reversed forks, as shown by electron microscopy[9]. After XPF-dependent unhooking of the reversed structure[9,50], double-strand DNA break repair generates joining products that barely enter the gel[51] (Fig. 1b, well product). Some of these species are resolved into monomeric, supercoiled plasmids that represent the final, fully repaired product (Fig. 1b, SC) that is sensitive to SapI digestion. **c**, Intermediates generated during replication-coupled repair of an AP-ICL (pICL^{AP}). Top, progression through the NEIL3 repair pathway generates intermediates resulting from fork convergence, NEIL3-dependent *N*-glycosyl bond cleavage, nascent strand ligation, decatenation, and TLS. Bottom, deproteinization of the DNA intermediates depicted along the top yields DNA structures that travel with characteristic mobilities during native gel electrophoresis. These structures are indicated along the side of the gel and with coloured dots in Fig. 3a and other figures.

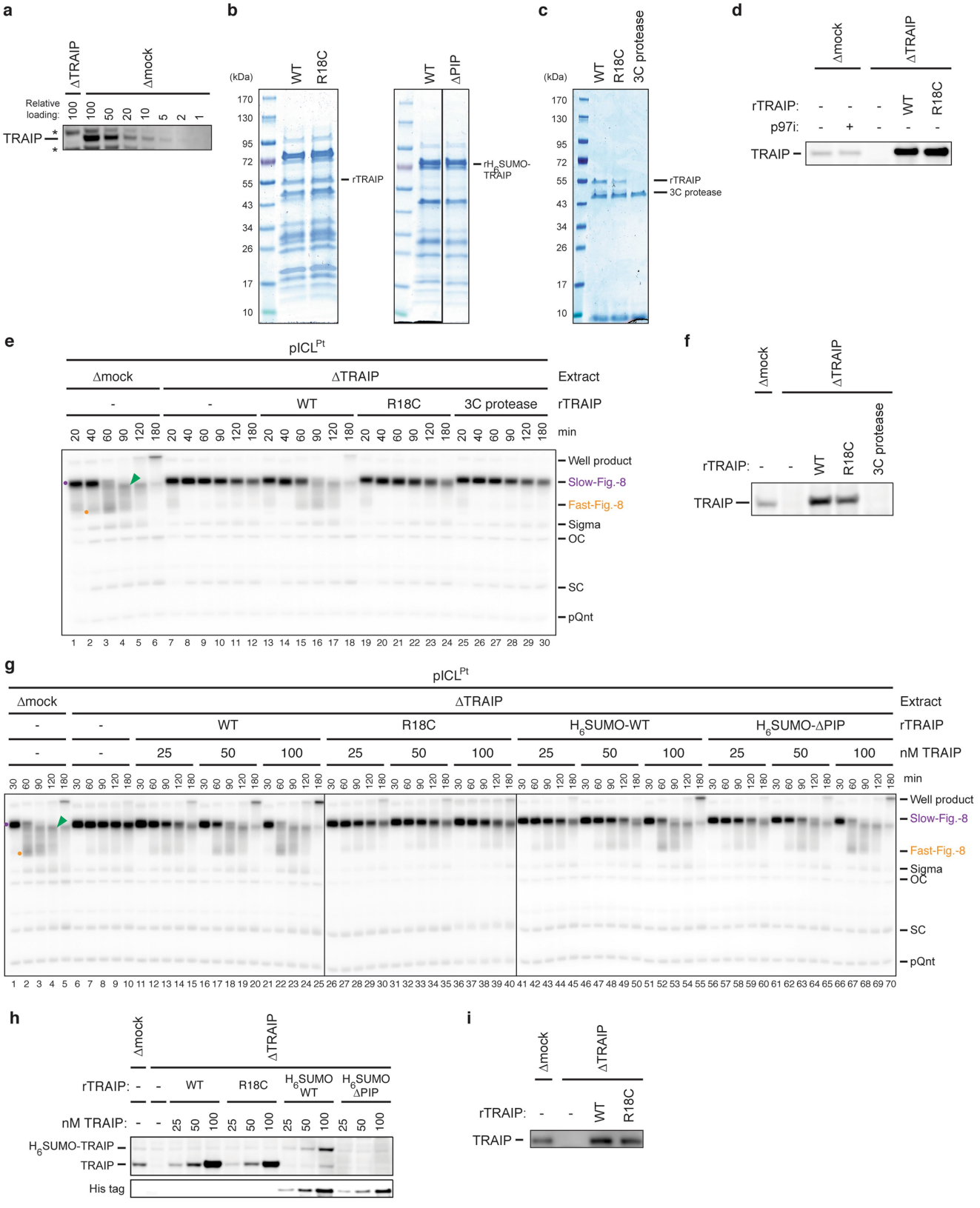

Extended Data Fig. 2 | See next page for caption.

Extended Data Fig. 2 | Recombinant TRAIP supports CMG unloading at cisplatin-ICLs. a, NPE immunodepleted of TRAIP was loaded alongside a dilution series of mock-depleted NPE and analysed for TRAIP. A relative loading amount of 100 corresponds to 2 μl of NPE. Non-specifically detected proteins are marked with asterisks. Four independent experiments. **b**, Bacterially expressed wild-type rTRAIP, rTRAIP(R18C), His_6-SUMO-rTRAIP(wild type), and His_6-SUMO-rTRAIP(ΔPIP) (comprising residues 1–455) were partially purified, resolved by SDS–PAGE and visualized with Coomassie blue staining. Note that His_6-SUMO-rTRAIP is obscured by co-migrating, contaminating proteins. Bacterially expressed rTRAIP was used for all subsequent experiments, unless otherwise indicated. Results are typical of at least two independent purifications. **c**, Wild-type rTRAIP and rTRAIP(R18C) were expressed in Sf9 insect cells and purified using an N-terminal 3×Flag tag. The tag was then cleaved using 3C protease. The recombinant proteins, along with a buffer sample containing 3C protease only, were resolved by SDS–PAGE and visualized with Coomassie blue staining. Results are typical of at least three independent purifications. **d**, Mock-depleted and TRAIP-depleted extracts supplemented with wild-type rTRAIP or rTRAIP(R18C) used in Fig. 1b were analysed by immunoblotting for TRAIP. The absence of the non-specific bands seen in **a** may be due to shorter incubation with the TRAIP antibody. The concentration of added recombinant TRAIP relative to endogenous TRAIP fluctuates among experiments (for example, compare **d** and Extended Data Fig. 3b). We ascribe this difference to variations in non-specific removal of endogenous TRAIP from extracts during the mock-depletion procedure, and possibly also in the delivery of recombinant TRAIP into the extract. Seven independent experiments. **e**, $pICL^{Pt}$ was replicated in mock-depleted or TRAIP-depleted extracts supplemented with [α-^{32}P]dATP and Sf9-expressed wild-type rTRAIP, rTRAIP(R18C) or 3C protease alone and analysed as in Fig. 1b. Two independent experiments. **f**, Extracts used in the replication reaction shown in **e** were analysed as in **d**. Two independent experiments. **g**, $pICL^{Pt}$ was replicated in the indicated egg extracts with [α-^{32}P]dATP and analysed as in Fig. 1b. Two independent experiments. **h**, Extracts used in the replication reaction shown in **g** were analysed as in **d**. Note that deleting the C-terminal PIP box disrupts the epitope for the TRAIP antibody used for immunoblotting. Therefore, to assess the activity of TRAIP(ΔPIP) in ICL repair relative to wild-type TRAIP, His_6-SUMO-tagged proteins were added back to TRAIP-depleted extract and assayed in **g**. The relative amounts of His_6-SUMO-TRAIP(wild type) and His_6-SUMO-TRAIP(ΔPIP) were compared by detecting the histidine tag. By blotting the same extracts for TRAIP, a comparison of the relative concentrations of His_6-SUMO-TRAIP(ΔPIP) and endogenous TRAIP was made. Two independent experiments. **i**, Mock-depleted and TRAIP-depleted extracts used in the replication reactions shown in Fig. 1c, d were analysed as in **d**. Three independent experiments.

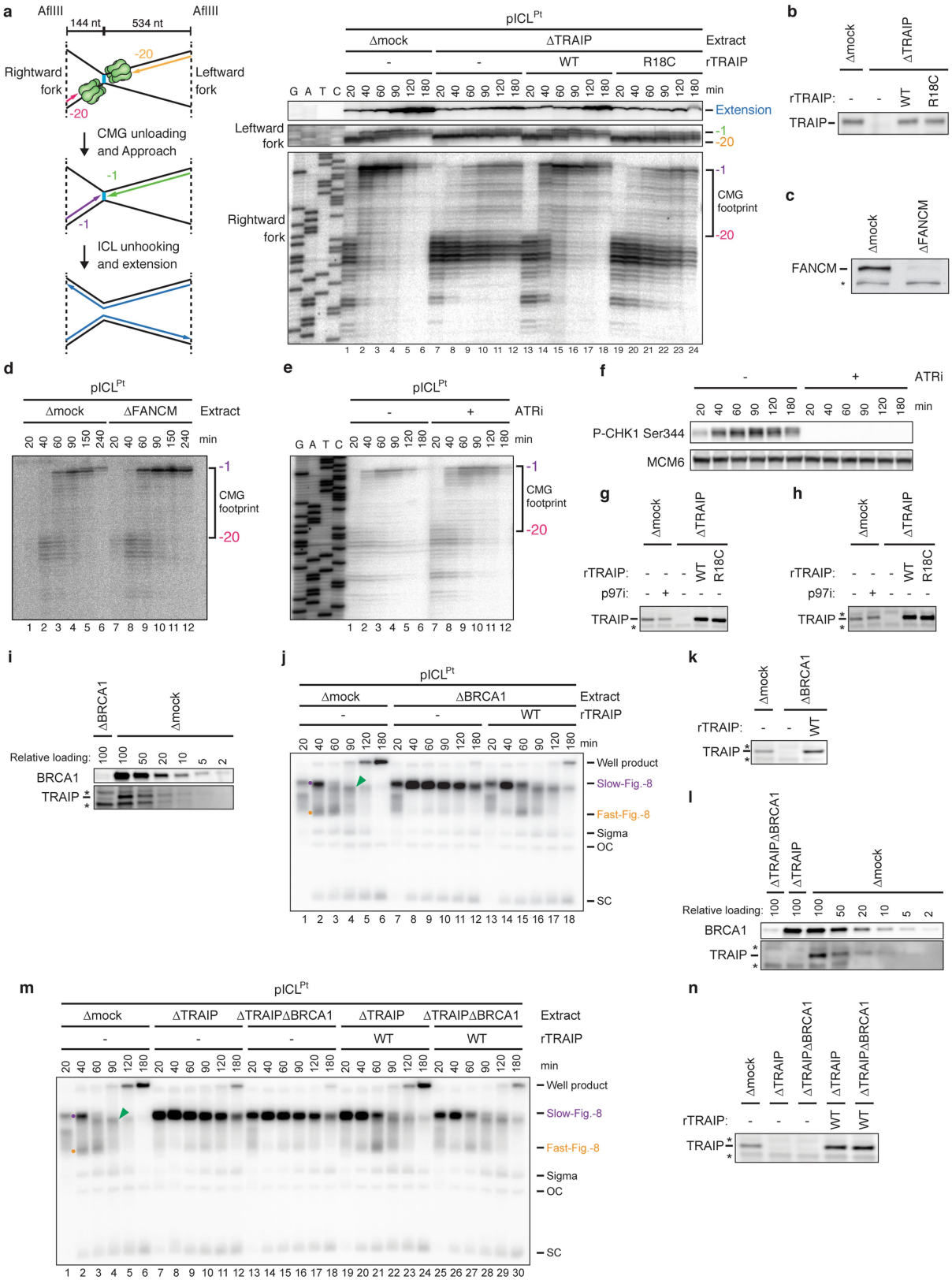

Extended Data Fig. 3 | See next page for caption.

Extended Data Fig. 3 | TRAIP, but not FANCM, ATR or BRCA1, is required for CMG unloading at cisplatin-ICLs. a, Left, schematic of nascent strands generated at ICLs. When forks converge on an ICL, nascent strands stall about 20 nucleotides from the ICL on either side of the lesion owing to the footprint of CMG (green hexamer). AflIII cuts 144 nucleotides to the left and 534 nucleotides to the right of the ICL, generating characteristic products for the leftward and rightward leading strands upon fork convergence, CMG unloading, and leading strand extension. Right, nascent strand analysis of $pICL^{Pt}$ replication in the indicated extracts. After replication with [α-^{32}P]dATP, nascent strands were extracted, digested with AflIII and resolved on a denaturing polyacrylamide gel alongside a sequencing ladder and visualized by autoradiography. As seen previously[2,52], when replication forks converged on the ICL in mock-depleted egg extracts, leading strands initially stalled 20–40 nucleotides from the lesion (lane 1) and then advanced to the −1 position (lanes 2–6), which depends on CMG dissociation[21,52]. By contrast, in TRAIP-depleted egg extracts, the −20 footprint persisted for three hours (lanes 7–12). This effect was rescued with wild-type rTRAIP but not rTRAIP(R18C) (lanes 13–24). Two independent experiments. **b**, Extracts used in the replication reaction shown in **a** were analysed for TRAIP. Two independent experiments. **c**, Mock-depleted or FANCM-depleted extracts were analysed for FANCM. A non-specifically detected protein is marked with an asterisk. Two independent experiments. **d**, Nascent strand analysis of $pICL^{Pt}$ replicating in mock-depleted or FANCM-depleted extracts was performed as in **a**. The CMG footprint disappeared at the ICL in FANCM-depleted egg extract, consistent with FANCM not being required for CMG unloading at ICLs. Two independent experiments. **e**, $pICL^{Pt}$ was replicated in the absence or presence of ATR inhibitor ETP-46464 (ATRi), and nascent strand analysis was performed as in **a**. ATR inhibitor was added to the reaction 2.5 min after initiation. The CMG footprint disappeared at the ICL with or without ATR inhibitor, indicating that ATR signalling is not required for CMG unloading at ICLs. Two independent experiments. **f**, Extracts used in **e** were sampled at various time points and analysed for *Xenopus* CHK1 serine-344 phosphorylation to verify ATR inhibition. MCM6 was detected as a loading control. Two independent experiments. **g**, **h**, Mock-depleted and TRAIP-depleted extracts used in one of the replicate reactions quantified in Fig. 1e (**g**) and Fig. 1f (**h**) were analysed for TRAIP. Two independent experiments were performed for **g** and three independent experiments were performed for **h**. **i**, We previously showed that the immunodepletion of BRCA1 from egg extracts inhibits CMG unloading at ICLs, but this defect could not be rescued with recombinant BRCA1–BARD1 complex[8,21]. To test whether TRAIP is co-depleted with BRCA1, NPE was immunodepleted of BRCA1 with BRCA1 antiserum, loaded alongside a dilution series of mock-depleted NPE, and analysed for BRCA1 and TRAIP. A relative loading amount of 100 corresponds to 2 μl of NPE. Non-specifically detected proteins are marked with asterisks. This analysis revealed that immunodepletion of BRCA1 also removed TRAIP from NPE. We also observed TRAIP co-depletion with antibodies against other proteins (data not shown), suggesting that it interacts non-specifically with different antibodies. Two independent experiments. **j**, The extracts described in **i** were supplemented with $pICL^{Pt}$, [α-^{32}P]dATP and rTRAIP, as indicated, and analysed as in Fig. 1b. Wild-type rTRAIP suppressed the stabilization of the slow-figure-8 species seen in BRCA1-depleted extract, consistent with the restoration of CMG unloading, and indicating that the unloading defect seen in BRCA1-depleted egg extracts is due primarily to the removal of TRAIP from the extract. Two independent experiments. **k**, The extracts used in **j** were analysed for TRAIP. Two independent experiments. **l**, To determine whether BRCA1 contributes to TRAIP-dependent CMG unloading, NPE was immunodepleted of TRAIP or TRAIP and BRCA1 using Protein A Sepharose-purified antibodies purified from antiserum. A dilution series of mock-depleted NPE was loaded alongside the depleted extracts, and extracts were analysed for BRCA1 and TRAIP. A relative loading amount of 100 corresponds to 2 μl of NPE. Two independent experiments. **m**, The extracts described in **l** were supplemented with $pICL^{Pt}$, [α-^{32}P]dATP and rTRAIP, as indicated, and analysed as in Fig. 1b. Wild-type rTRAIP suppressed the accumulation of slow-figure-8 species to a similar extent in TRAIP-depleted egg extracts whether or not BRCA1 was co-depleted (lanes 19–30), indicating that BRCA1 is not needed to support TRAIP function. BRCA1 depletion reproducibly resulted in a decrease in well-product formation, suggesting a role for BRCA1 in recombination after a double-strand break is formed by ICL-unhooking incisions. Two independent experiments. **n**, The extracts used in **m** were analysed for TRAIP. Two independent experiments.

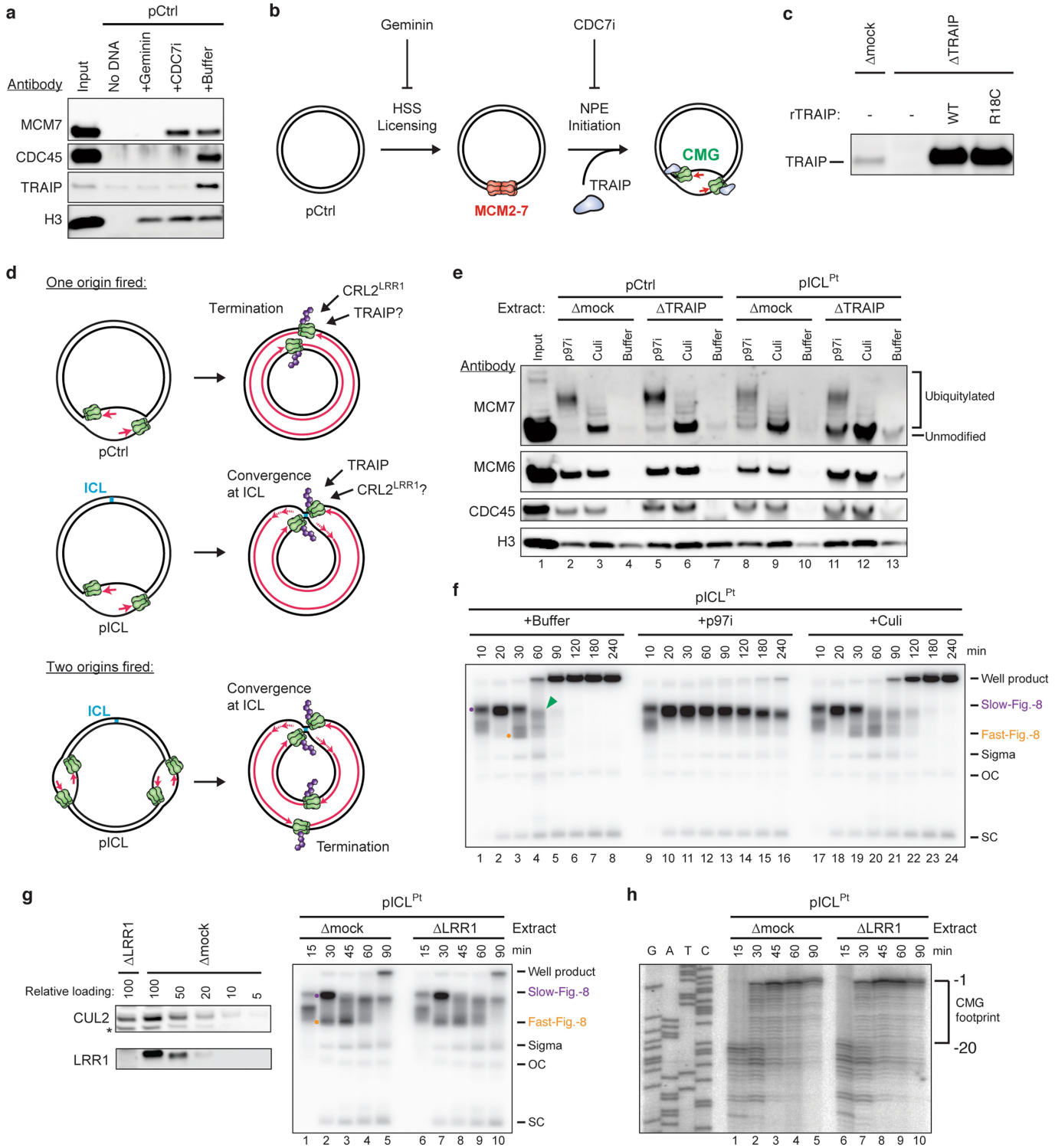

Extended Data Fig. 4 | See next page for caption.

Extended Data Fig. 4 | TRAIP and CRL2^{LRR1} promote distinct CMG unloading pathways. a, pCtrl was replicated in NPE in the presence of Geminin or the CDC7 inhibitor PHA-767491 (CDC7i). Eight minutes after the addition of NPE, the plasmid was recovered and the indicated proteins were analysed by immunoblot. Three independent experiments. **b**, Cartoon depicting the effects of Geminin and CDC7i, and the step at which TRAIP is recruited to chromatin. **c**, Extracts used in the replication reaction shown in Fig. 2e were analysed for TRAIP. Four independent experiments. **d**, Top, upon termination of pCtrl replication, CMG (green) unloading depends on CRL2^{LRR1}-mediated MCM7 ubiquitylation (purple)[23,53], but it is not known whether unloading also requires TRAIP. Middle, CMGs that have converged at an ICL undergo TRAIP-dependent ubiquitylation (Fig. 1), but the involvement of CRL2^{LRR1} is unknown. Bottom, if two origins fire on a single plasmid, one pair of replication forks converges at the ICL and undergoes TRAIP-dependent CMG unloading, whereas a second pair undergoes CRL2^{LRR1}-dependent unloading. Because both pairs of CMGs should undergo ubiquitylation, in some experiments we include Culi to monitor only TRAIP-dependent ubiquitylation. **e**, To determine whether TRAIP is required for CMG unloading during replication termination, we analysed proteins associated with plasmids 60 min after replication initiation in mock-depleted or TRAIP-depleted extracts containing p97i or Culi, as indicated. Chromatin was recovered and analysed for the indicated proteins. CMG unloading from pCtrl was unaffected by TRAIP depletion (compare lanes 4 and 7). Consistent with this, in the presence of p97i, TRAIP was not required for MCM7 ubiquitylation on pCtrl (compare lanes 2 and 5). By contrast, in the absence of TRAIP, CMG unloading from pICL^{Pt} was inhibited compared to the mock-depleted control (compare lanes 10 and 13), consistent with Fig. 1c. Similarly, TRAIP was essential for efficient MCM7 ubiquitylation on pICL^{Pt} (compare lanes 8 and 11, note the greater level of unmodified MCM7 in lane 11). The partial CMG unloading (lane 13) and residual MCM7 ubiquitylation observed on pICL^{Pt} in the absence of TRAIP (lane 11) were probably the result of termination events that occurred elsewhere on the plasmid (as described in **d**, bottom). Consistent with this interpretation, the combination of TRAIP depletion and Culi abolished MCM7 ubiquitylation (lane 12). Three independent experiments. **f**, To determine whether CRL2^{LRR1} contributes to CMG unloading at ICLs, pICL^{Pt} was replicated in undepleted extract containing p97i or Culi and analysed as in Fig. 1b. Culi had no effect on the accumulation of fast-figure-8 structures, consistent with CRL2^{LRR1} being dispensable for CMG unloading at ICLs. Two independent experiments. **g**, Left, to assess the effect of LRR1 depletion on CMG unloading at ICLs, NPE was immunodepleted of LRR1, loaded alongside a dilution series of mock-depleted NPE, and analysed for LRR1 and CUL2. A relative loading amount of 100 corresponds to 2 μl of NPE. Non-specifically detected protein is marked with an asterisk. Right, pICL^{Pt} was replicated in mock-depleted or LRR1-depleted egg extracts and analysed as in Fig. 1b. The absence of LRR1 had no effect on the formation of fast-figure-8 structures, supporting the idea that CRL2^{LRR1} is dispensable for CMG unloading at ICLs. Two independent experiments. **h**, Nascent strand analysis of pICL^{Pt} replicating in mock-depleted or LRR1-depleted extracts was performed as in Extended Data Fig. 3a. The CMG footprint disappeared with normal kinetics at the ICL in LRR1-depleted egg extract, consistent with CRL2^{LRR1} not being required for CMG unloading at ICLs. Two independent experiments.

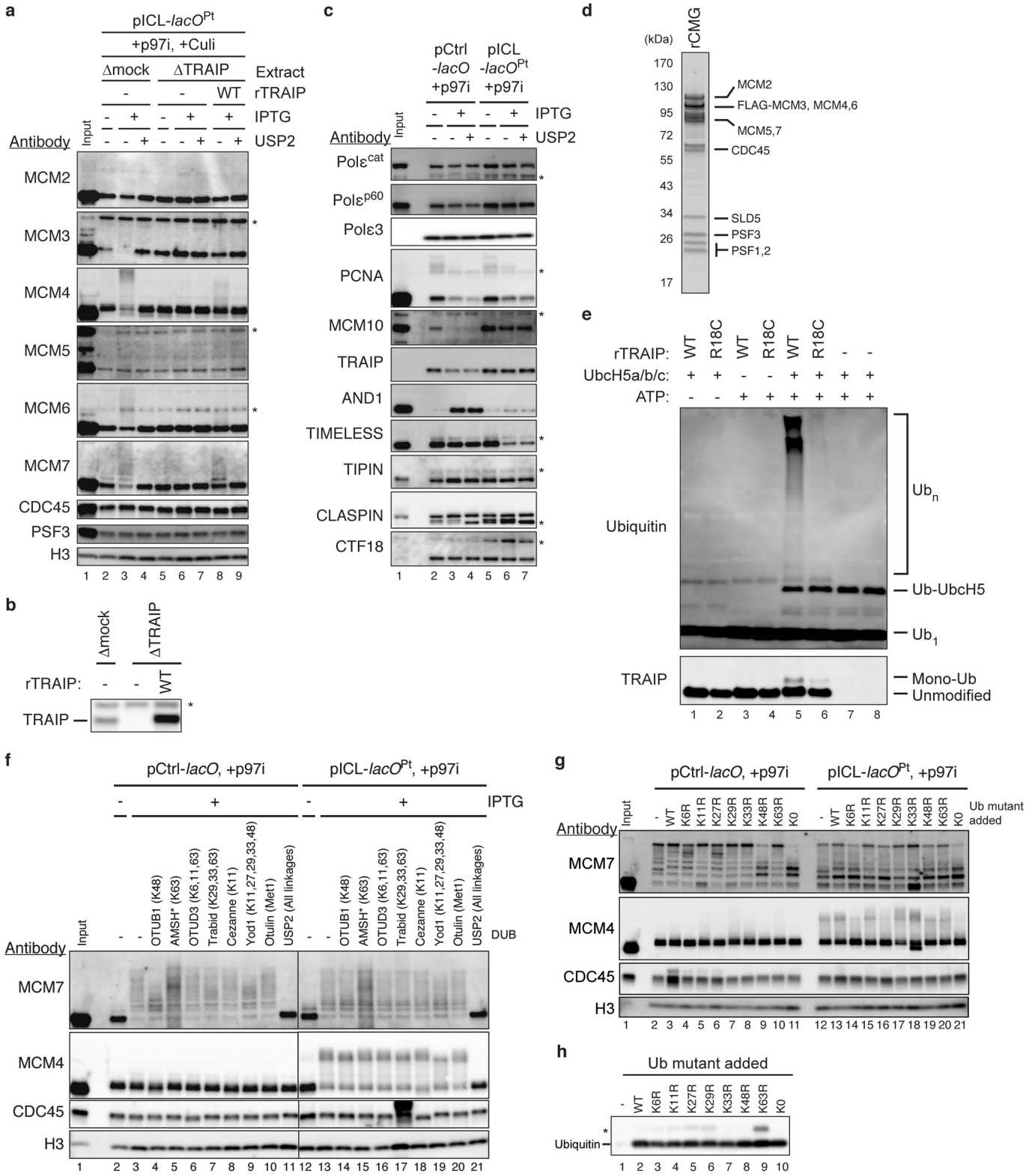

Extended Data Fig. 5 | See next page for caption.

Extended Data Fig. 5 | TRAIP ubiquitylates numerous CMG subunits with heterotypically linked chains upon fork convergence at an ICL. a, pICL-*lacO*^{Pt} was incubated with LacR before replication in mock- or TRAIP-depleted extracts. After 1 h of replication (to allow for termination of replication forks that do not converge on the ICL or *lacO* array as depicted in Figs. 2c), 0.3 mM NMS-873 was added and the extracts were incubated for 5 min to inhibit p97. IPTG (10 mM) and Sf9-expressed wild-type rTRAIP were then added as indicated and the extract was incubated for 2 h to disrupt LacR DNA binding and allow fork convergence and TRAIP-dependent ubiquitylation. The plasmid was recovered and analysed for the indicated proteins. Two independent experiments. **b**, The extracts described in **a** were analysed for TRAIP. Two independent experiments. **c**, pICL-*lacO*^{Pt} was incubated with LacR before replication in undepleted egg extracts. After 30 min of replication (to allow for termination of replication forks that do not converge on the ICL or *lacO* array as depicted in Figs. 2c), 0.3 mM NMS-873 was added and the extracts were incubated for 5 min to inhibit p97. IPTG (10 mM) was then added as indicated to disrupt LacR DNA binding and the extract was incubated for 1 h to allow for fork convergence. The plasmid was recovered and analysed for the indicated proteins. Two independent experiments. **d**, Recombinant CMG was purified, resolved by SDS–PAGE, and visualized with SYPRO Ruby staining. Results are typical of at least five independent purifications. **e**, rTRAIP ubiquitin ligase activity. Wild-type rTRAIP or rTRAIP(R18C) was combined with ubiquitin, E1 ligase, three E2 ligases (UbcH5a, UbcH5b, UbcH5c) and ATP as indicated. Polyubiquitin chain synthesis (top) and TRAIP autoubiquitylation (bottom) were detected by immunoblotting the reactions with ubiquitin and TRAIP antibody, respectively. rTRAIP(R18C) was much more compromised in forming free polyubiquitin chains in this assay than it was in ubiquitylating rCMG (see Fig. 2d). The data suggest that the interaction between TRAIP and CMG can suppress, to a great extent, the profound ubiquitylation defect of the R18C mutation. Three independent experiments. **f**, pCtrl-*lacO* and pICL-*lacO*^{Pt} were replicated in undepleted extract as in **c** and recovered. Samples were treated with the indicated DUBs and analysed for the indicated proteins. Three independent experiments. **g**, pCtrl-*lacO* and pICL-*lacO*^{Pt} pre-bound with LacR were replicated in undepleted extract as in **c**. At the time of IPTG addition to release the LacR array and allow for fork convergence, 100 μM recombinant ubiquitin (wild-type or various lysine-to-arginine mutants) was added to the extract (which contains around 8 μM endogenous ubiquitin) and incubated for 1 h. The plasmid was recovered and analysed for the indicated proteins. Three independent experiments. **h**, Extracts used in **g** were analysed for ubiquitin. Some ubiquitin mutants contain a di-ubiquitin species (marked with an asterisk). Whether this arises upon addition to the extract is unclear. Three independent experiments.

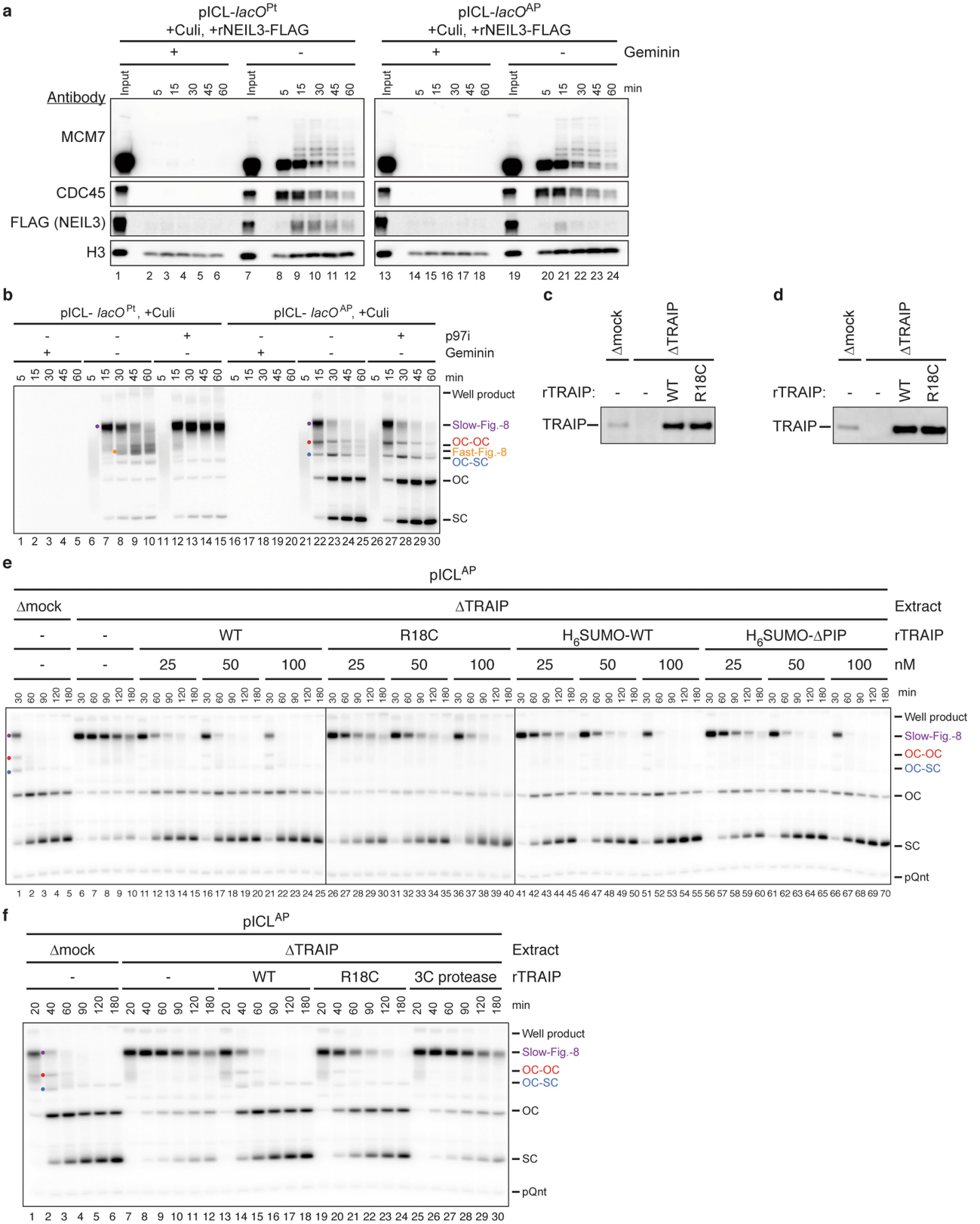

Extended Data Fig. 6 | AP-ICL repair by NEIL3 requires TRAIP. **a**, Analysis of chromatin-associated proteins during replication of pICL-*lacO*^{Pt} or pICL-*lacO*^{AP} in undepleted extract in the presence and absence of Geminin, as indicated. At different times after replication initiation, chromatin was recovered and analysed for the indicated proteins. Two independent experiments. **b**, pICL-*lacO*^{Pt} and pICL-*lacO*^{AP} were replicated in undepleted extract supplemented with Culi, Geminin and p97i, as indicated, and analysed as in Fig. 1b. Two independent experiments. **c**, The extracts used in the replication reaction shown in Fig. 3a were analysed for TRAIP. Five independent experiments. **d**, Extracts used in one of the reactions quantified in Fig. 3b were analysed as in **c**. Three independent experiments. **e**, **f**, pICL^{AP} was replicated in the extracts shown in Extended Data Fig. 2h (**e**) and Extended Data Fig. 2f (**f**) with [α-^{32}P]dATP and analysed as in Fig. 1b. Two independent experiments were performed for **e** and **f**.

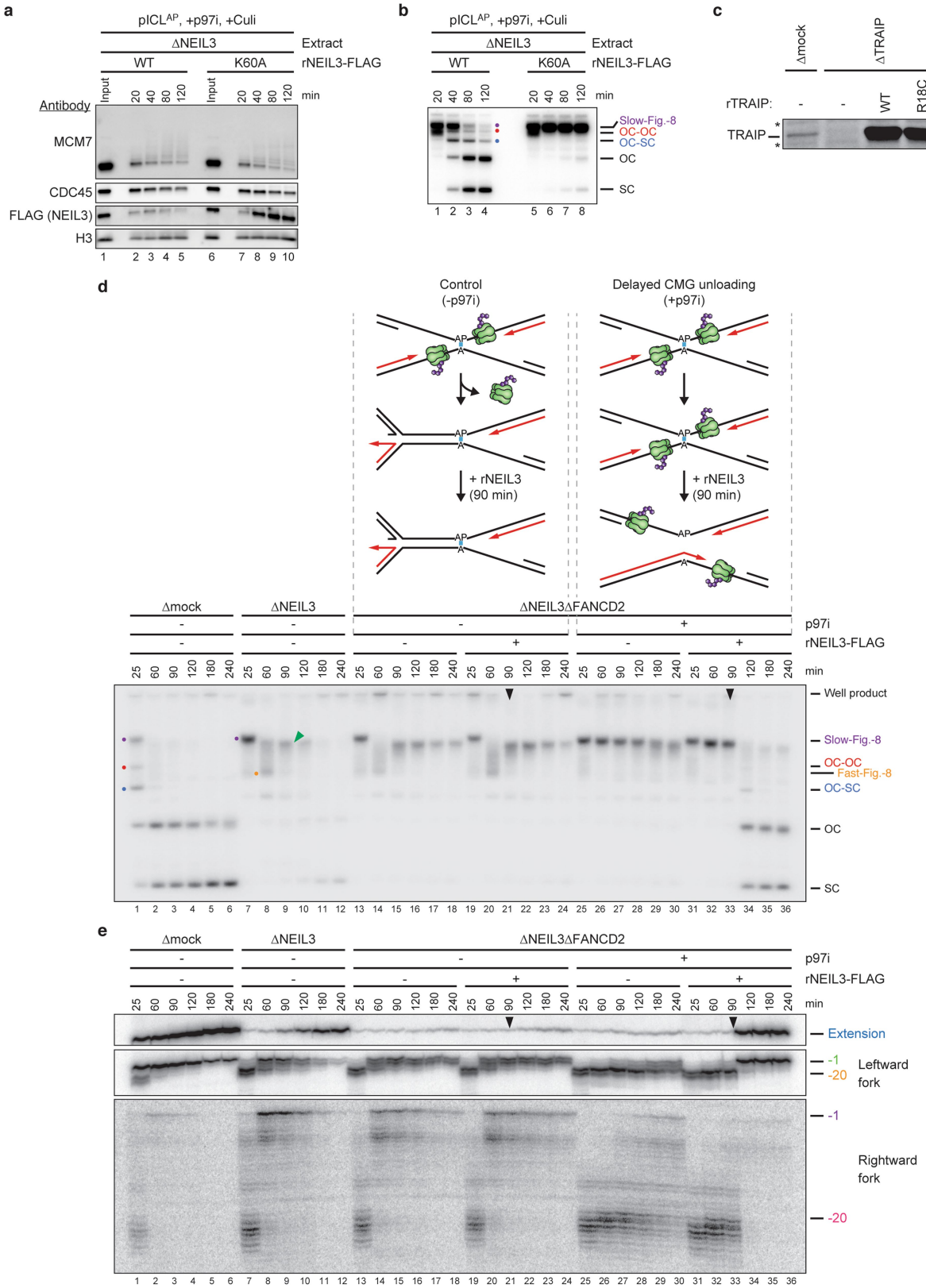

Extended Data Fig. 7 | See next page for caption.

Extended Data Fig. 7 | ICL repair by NEIL3 requires the association of CMG with chromatin. a, Analysis of proteins associated with $pICL^{AP}$ during replication with NEIL3-depleted extract supplemented with wild-type rNEIL3 or catalytically inactive rNEIL3(K60A), p97i and Culi. At the indicated times after replication initiation, chromatin was recovered and analysed for the indicated proteins. Consistent with NEIL3 dissociating rapidly after unhooking, rNEIL3(K60A) was recovered more efficiently with $pICL^{AP}$ than was wild-type rNEIL3. Two independent experiments. **b**, $pICL^{AP}$ was replicated with NEIL3-depleted extract supplemented with wild-type rNEIL3 or rNEIL3(K60A), p97i and Culi, as indicated, and analysed as in Fig. 1b. Two independent experiments. **c**, The extracts used in Fig. 3c were analysed for TRAIP. Non-specifically detected proteins are marked with asterisks. Four independent experiments. **d**, If NEIL3 activity is coupled to ubiquitylated CMG, NEIL3 should function only before CMG has been unloaded. To test this prediction, we inhibited all unhooking events by depleting egg extracts of NEIL3 (to block the NEIL3 pathway) and FANCD2 (to block the Fanconi anaemia pathway). At a late time point (90 min), we added back rNEIL3 to extract in which CMG had been allowed to unload (−p97i), or extract in which CMG unloading was prevented (+p97i). Our model predicts that rNEIL3 should unhook the ICL only in the latter setting. Top, schematic illustrating the late addition of rNEIL3 to NEIL3-depleted and FANCD2-depleted egg extracts in the absence (left) or presence (right) of p97i. Bottom, replication of $pICL^{AP}$ in mock-depleted, NEIL3-depleted, or both NEIL3- and FANCD2-depleted extracts in the presence of [α-^{32}P]dATP. Extracts were supplemented with p97i as indicated and rNEIL3 was added at 90 min where indicated (black arrowheads). Replication intermediates were resolved and visualized as in Fig. 1b. Depletion of NEIL3 and FANCD2 blocked all unhooking of the AP-ICL, resulting in an accumulation of reversed forks (lane 9, green arrowhead). Addition of rNEIL3 at 90 min in the absence of p97i (after CMG unloading) failed to induce unhooking, based on the persistence of the reversed forks (lanes 21–24). By contrast, when CMG unloading was prevented with p97i (lanes 25–30; note the persistence of slow-figure-8 intermediates), late rNEIL3 addition led to efficient ICL unhooking, as seen from the rapid conversion of slow-figure-8 intermediates to open circular and supercoiled species (lanes 34–36). This gel image has been compressed vertically to fit the page. Two independent experiments. **e**, To confirm the presence or absence of CMG at the AP-ICL, DNA was recovered from the reactions described in **d** and subjected to nascent strand analysis as in Extended Data Fig. 3a. Top, extension products and nascent strands of the leftward fork. Bottom, nascent strands of the rightward fork. Black arrowheads, rNEIL3 addition. Depletion of NEIL3 and FANCD2 did not affect loss of the CMG footprint at −20 and caused persistence of nascent DNA strands at −1 (lanes 13–24), which is indicative of failure to unhook the ICL. Late addition of NEIL3 failed to stimulate further nascent strand extension (lanes 21–24), indicating that unhooking did not occur. Treatment with p97i led to persistence of the CMG footprint at −20 (lanes 25–30), consistent with retention of CMG at the ICL, and late addition of NEIL3 stimulated formation of full-length nascent strand extension products (lanes 34–36), indicative of efficient unhooking. Taken together, the data in **d** and **e** strongly suggest that NEIL3 activity is coupled to the presence of CMG at the site of the ICL, although we cannot rule out that NEIL3 activity is suppressed by downstream events, such as fork reversal, that depend on CMG unloading. Two independent experiments.

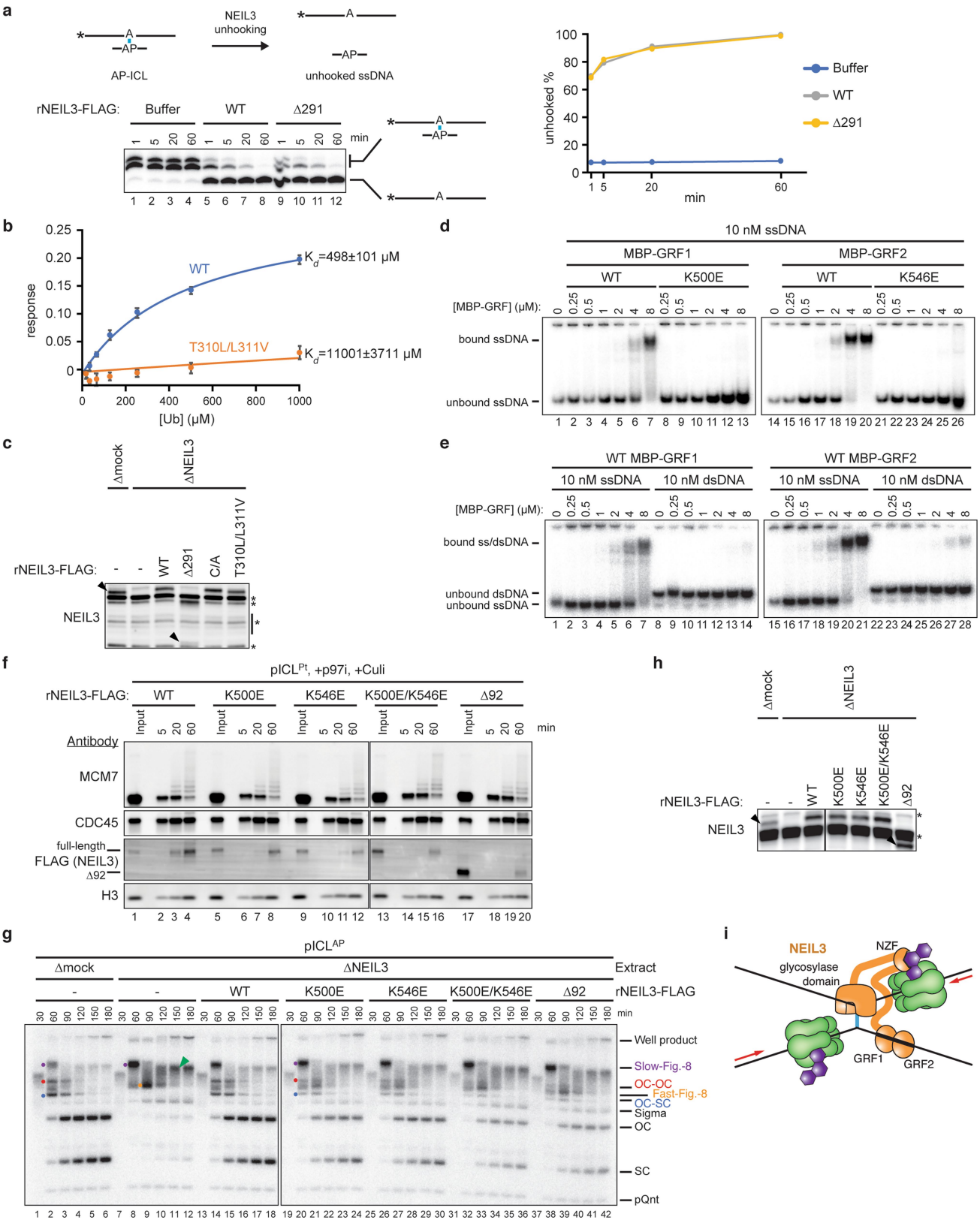

Extended Data Fig. 8 | See next page for caption.

Extended Data Fig. 8 | The zinc-finger domains of NEIL3 contribute to its recruitment to the replication fork. a, Left, to determine whether rNEIL3(Δ291) is catalytically active, a model AP-ICL substrate comprising a synthetic 5′-radiolabelled 24mer oligonucleotide crosslinked to a ~3mer was mixed with rNEIL3(Δ291) or wild-type rNEIL3. Crosslinked and unhooked species were resolved by denaturing polyacrylamide gel electrophoresis and visualized by autoradiography. Asterisks indicate the ^{32}P radiolabel. Note that the crosslinked species migrates as a doublet owing to heterogeneity in the bottom strand after RNase digestion (see Methods for details). Right, quantification of unhooking. Equivalent results were obtained in three independent experiments, which show that rNEIL3(Δ291) retains full glycosylase activity. **b**, Interaction of the NEIL3 NPL4-type zinc-finger (residues 300–328) with ubiquitin. GST-NEIL3 NZF fusion protein (wild-type or T310L/L311V-substituted) was immobilized on a biosensor tip and monoubiquitin binding was measured by biolayer interferometry. The ubiquitin binding response was corrected for non-specific binding to GST and plotted as a function of ubiquitin concentration. Data are mean ± s.e.m. from three independent experiments. **c**, Extracts used in Fig. 3e were analysed for NEIL3. Black arrowheads, NEIL3-specific bands. rNEIL3$^{\Delta 291}$ is not efficiently detected by the NEIL3-specific primary antibody. Non-specifically detected proteins are marked with asterisks. Three independent experiments. **d**, **e**, To test whether the two GRF zinc-fingers in NEIL3 interact with ssDNA, we expressed each individually and performed electrophoretic mobility shift assays. rMBP-NEIL3 GRF zinc-finger fusion proteins (wild-type or substituted) were incubated with 5′-radiolabelled 25-mer ssDNA or dsDNA. Bound and unbound DNAs were resolved by native PAGE and visualized by autoradiography. This analysis reveals that both GRF domains bind specifically to ssDNA. Two independent experiments were performed for **d** and **e**. **f**, Analysis of proteins associated with pICL^{Pt} during replication in undepleted extract in the presence of p97i and Culi. Extracts were supplemented with wild-type or mutated rNEIL3. At different times, chromatin was recovered and analysed for the indicated proteins. The individual GRF substitutions modestly affected recovery of rNEIL3 upon pICL pull-down while combination of the substitutions or deletion of both GRF zinc-fingers strongly reduced rNEIL3 recovery, indicating that interactions mediated by the GRF zinc-fingers promote recruitment of NEIL3 to an ICL. Two independent experiments. **g**, pICL^{AP} was replicated in mock-depleted or NEIL3-depleted extracts supplemented with wild-type or mutated NEIL3 as indicated and analysed as in Fig. 1b. Relative to wild-type rNEIL3, rNEIL3 with substitutions in either GRF zinc-finger that abolish ssDNA binding (K500E and K546E) exhibited modest defects in pICL^{AP} unhooking that were exacerbated when the substitutions were combined, indicating that interactions between the GRF zinc-fingers and ssDNA contribute to ICL repair. Two independent experiments. **h**, Extracts used in the replication reactions shown in **g** were analysed for NEIL3. Non-specifically detected proteins are marked with asterisks. Two independent experiments. **i**, Model for recruitment of NEIL3 to chromatin by zinc-finger-mediated interactions. Upon replication-fork convergence at an ICL, TRAIP-dependent CMG ubiquitylation recruits NEIL3 through direct interactions between the NZF domain of NEIL3 and ubiquitin. Association of NEIL3 with chromatin is further enhanced by interactions between the tandem GRF zinc-fingers and ssDNA, possibly on the lagging strand template.

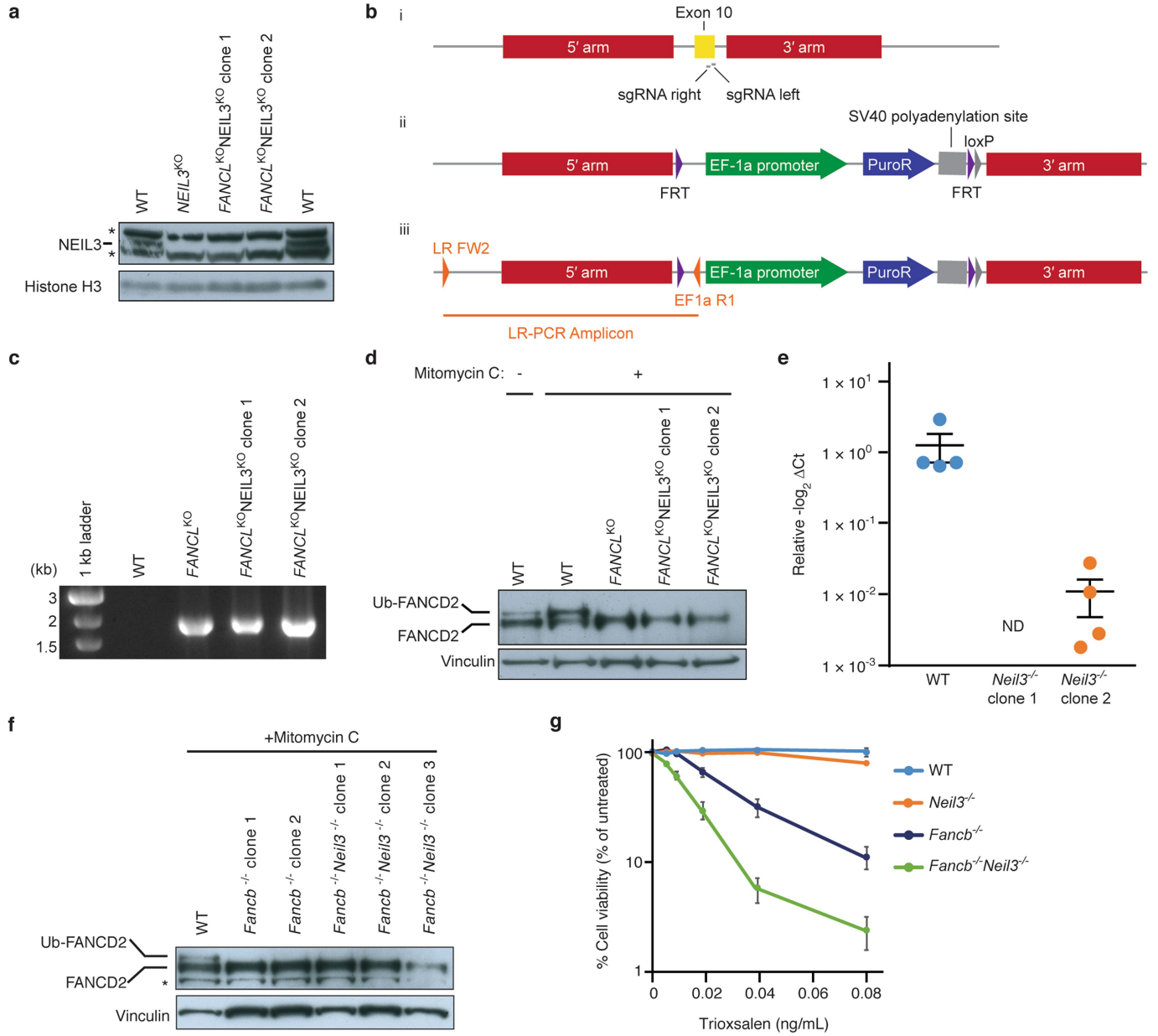

Extended Data Fig. 9 | Knockout of the Fanconi anaemia and NEIL3 pathways have additive effects on ICL sensitivity in mammalian cells. **a**, Immunoblot analysis of NEIL3 expression in wild-type, *NEIL3*-knockout and *FANCL*/*NEIL3*-knockout HAP1 cell lines. Histone H3 was detected as a loading control. Non-specifically detected proteins are marked with asterisks. Analysis performed twice. **b**, Schematic of *FANCL* targeting by CRISPR. (i) Human *FANCL* exon 10, single-guide (sg)RNA binding sites, and homology arm targets; (ii) *FANCL*-Puro targeting construct with homology arms flanking exon 10; (iii) Targeted *FANCL* allele with integrated puromycin-resistance cassette. **c**, Detection of the integrated puromycin-resistance cassette in HAP1 cells by *FANCL* long-range PCR. Analysis performed twice. **d**, Analysis of FANCD2 ubiquitylation in mitomycin-C-treated wild-type, *FANCL*-knockout and *FANCL*/*NEIL3*-knockout HAP1 cell lines to confirm *FANCL* knockout. Vinculin was detected as a loading control. FANCL is the catalytic subunit of the Fanconi anaemia core complex, which ubiquitylates FANCD2. Analysis performed twice. **e**, *Neil3* qRT–PCR confirming gene disruption in CH12 cell lines. ND, not detected. Analysis performed once. **f**, Analysis of FANCD2 ubiquitylation in mitomycin-C-treated *Fancb*-knockout and *Neil3*/*Fancb*-knockout CH12 cell lines to confirm *Fancb* knockout. Vinculin was detected as a loading control. A non-specifically detected protein is marked with an asterisk. Analysis performed once. **g**, Cell viability of wild-type, *Fancb*-knockout, *Neil3*-knockout or *Fancb*/*Neil3*-knockout CH12 cells after exposure to trioxsalen and UVA irradiation. Two independent clones were used for the single mutants and three independent clones were used for the double mutant. Data are mean ± s.e.m. We speculate that, relative to HAP1 cells, CH12 cells may be more reliant on the Fanconi anaemia pathway to repair trioxsalen-induced damage owing to lower expression levels of NEIL3. Three independent experiments.

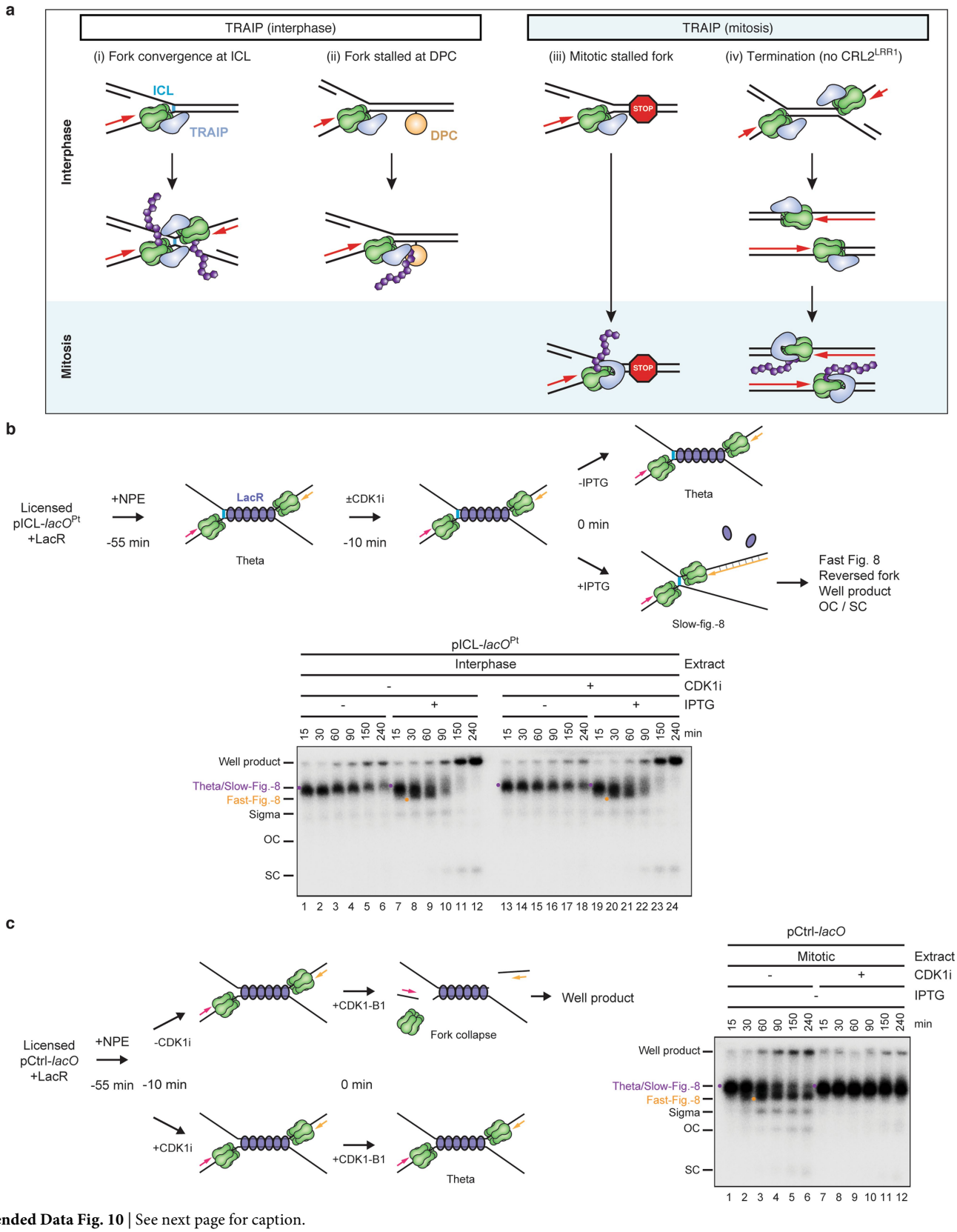

Extended Data Fig. 10 | See next page for caption.

Extended Data Fig. 10 | Model of the action of TRAIP in interphase and mitosis. a, TRAIP (blue) travels with the replisome and associates with CMG, directly or indirectly (i–iv, top). In interphase, TRAIP is oriented such that its E2 (the identity of which is unknown) points ahead of the replisome. As a result, TRAIP cannot ubiquitylate the CMG it is associated with, but it can ubiquitylate any protein that lies in the path of the replisome. TRAIP can thus ubiquitylate CMG *in trans* when two replisomes meet (i), and it can ubiquitylate DPCs that block the path of the replisome (ii). We speculate that TRAIP ubiquitylates any proteinaceous structure that causes extended stalling of the replisome. In mitosis, TRAIP undergoes a conformational change so that it can ubiquitylate the CMG with which it is associated *in cis*. As a result, in mitosis, stalled forks undergo TRAIP-dependent CMG ubiquitylation in the absence of fork convergence (iii)[4]. We propose that TRAIP does not ubiquitylate terminated CMGs in interphase because they rapidly move past each other[30], precluding ubiquitylation by the forward-pointing TRAIP (iv, middle). However, upon mitotic entry, terminated CMGs undergo TRAIP-dependent ubiquitylation *in cis* (iv, bottom)[4]. It is notable that TRAIP-dependent CMG unloading in interphase egg extracts is not dependent on residual CDK1 activity (**b**, **c**), which indicates that TRAIP is regulated differently in interphase and mitosis. **b**, In interphase egg extracts, TRAIP travels with DNA replication forks but ubiquitylates CMGs only when forks converge. In the presence of cyclin B1-CDK1, TRAIP is activated in the absence of fork convergence[4] (summarized in **a**). We therefore wanted to know whether TRAIP-dependent CMG unloading in interphase egg extract depends on residual CDK1 activity. Top, reaction scheme to determine whether the action of TRAIP at ICLs in interphase egg extract requires residual CDK1 activity. Replication of pICL-*lacO*^{Pt} with a pre-assembled LacR array was initiated by addition of NPE (−55 min). Forty-five minutes after initiation (−10 min), reactions were supplemented with buffer or the CDK1 inhibitor RO-3306 (CDK1i) and allowed to incubate for an additional 10 min; CDK1i was added late to avoid inhibition of replication initiation. The LacR array was then released with the addition of IPTG to trigger fork convergence and ICL repair (0 min). In a control, buffer instead of IPTG was added to maintain the LacR array and thereby prevent fork convergence. At the indicated times after IPTG addition, samples were collected and analysed as in Fig. 1b to look for evidence of CMG unloading and ICL processing. Bottom, experiment described in top scheme. Fork stalling at the boundaries of the LacR array lead to a theta structure (lanes 1, 7, 13, 19). Upon addition of IPTG, theta was converted to slow-figure-8, fast-figure-8 (co-migrating with theta) and well products with equal efficiency in the presence and absence of CDK1i (compare lanes 7–12 and 19–24). The data suggest that CDK1 is not required for CMG unloading or ICL repair. Two independent experiments. **c**, Left, reaction scheme of a control experiment to ensure that the addition of CDK1i in **b** blocked CDK1 activity. As recently described[4], when replication forks are stalled at a LacR array, the subsequent addition of cyclin B1-CDK1 promotes TRAIP-dependent CMG unloading and fork breakage, alternative end joining, and the formation of aberrant replication products that migrate in the well of an agarose gel. To verify that CDK1 was effectively inhibited in **a**, we used this CDK1-dependent well-product formation as an assay. To this end, replication of pCtrl-*lacO* with a pre-assembled LacR array was initiated (−55 min) by addition of NPE. Forty-five min after initiation (−10 min), reactions were supplemented with CDK1i or buffer and allowed to incubate for an additional 10 min. Cyclin B1-CDK1 was then added to activate fork breakage and well-product formation (0 min). Right, experiment described in left scheme. As expected, the addition of cyclin B1-CDK1 in the absence of CDK1i led to the formation of well products (lanes 25–30), but in the presence of CDK1i well products were not formed (lanes 31–36). Two independent experiments. Note that the experiments in **b** and **c** were performed in parallel; extracts were aliquoted for the various conditions described at 0 min. Therefore, the CDK1i effectively inhibited CDK1-dependent activation of TRAIP. We conclude that TRAIP activation at ICLs does not depend on residual CDK1 activity.

nature research

Corresponding author(s): Johannes C. Walter

Last updated by author(s): Jan 22, 2019

Reporting Summary

Nature Research wishes to improve the reproducibility of the work that we publish. This form provides structure for consistency and transparency in reporting. For further information on Nature Research policies, see Authors & Referees and the Editorial Policy Checklist.

Statistics

For all statistical analyses, confirm that the following items are present in the figure legend, table legend, main text, or Methods section.

n/a	Confirmed	
☐	☒	The exact sample size (*n*) for each experimental group/condition, given as a discrete number and unit of measurement
☐	☒	A statement on whether measurements were taken from distinct samples or whether the same sample was measured repeatedly
☒	☐	The statistical test(s) used AND whether they are one- or two-sided *Only common tests should be described solely by name; describe more complex techniques in the Methods section.*
☒	☐	A description of all covariates tested
☒	☐	A description of any assumptions or corrections, such as tests of normality and adjustment for multiple comparisons
☐	☒	A full description of the statistical parameters including central tendency (e.g. means) or other basic estimates (e.g. regression coefficient) AND variation (e.g. standard deviation) or associated estimates of uncertainty (e.g. confidence intervals)
☒	☐	For null hypothesis testing, the test statistic (e.g. *F*, *t*, *r*) with confidence intervals, effect sizes, degrees of freedom and *P* value noted *Give P values as exact values whenever suitable.*
☒	☐	For Bayesian analysis, information on the choice of priors and Markov chain Monte Carlo settings
☒	☐	For hierarchical and complex designs, identification of the appropriate level for tests and full reporting of outcomes
☒	☐	Estimates of effect sizes (e.g. Cohen's *d*, Pearson's *r*), indicating how they were calculated

Our web collection on statistics for biologists contains articles on many of the points above.

Software and code

Policy information about availability of computer code

Data collection	Autoradiograms were imaged with the Typhoon FLA 7000 utilizing the FujiFilm FLA 7000 version 1.12 user interface Immunoblots were imaged using the Amersham Imager 680.
Data analysis	Autoradiograms and immunoblots were analyzed using Image J version 1.52

For manuscripts utilizing custom algorithms or software that are central to the research but not yet described in published literature, software must be made available to editors/reviewers. We strongly encourage code deposition in a community repository (e.g. GitHub). See the Nature Research guidelines for submitting code & software for further information.

Data

Policy information about availability of data

All manuscripts must include a data availability statement. This statement should provide the following information, where applicable:

- Accession codes, unique identifiers, or web links for publicly available datasets
- A list of figures that have associated raw data
- A description of any restrictions on data availability

No datasets were generated or analyzed for this study.

Field-specific reporting

Please select the one below that is the best fit for your research. If you are not sure, read the appropriate sections before making your selection.

☒ Life sciences ☐ Behavioural & social sciences ☐ Ecological, evolutionary & environmental sciences

Life sciences study design

All studies must disclose on these points even when the disclosure is negative.

Sample size	No sample size calculations were performed. All experiments were performed at least twice with a representative result shown. Quantified results were from the number of replicates indicated in the Figure legends.
Data exclusions	No data were excluded from the analysis.
Replication	All attempts at replication were successful. Experiments were performed at least twice and key results were replicated independently by two and in some cases three different people.
Randomization	Randomization was not relevant to this study. For molecular biology studies, common extracts were subject to the indicated treatments. For colony survival cells from a common pool were treated with increasing levels of genotoxic agent.
Blinding	For electron microscopy experiments, the scorer was blinded to experimental conditions before counting pre-incision and reversed fork structures.

Reporting for specific materials, systems and methods

We require information from authors about some types of materials, experimental systems and methods used in many studies. Here, indicate whether each material, system or method listed is relevant to your study. If you are not sure if a list item applies to your research, read the appropriate section before selecting a response.

Materials & experimental systems

n/a	Involved in the study
☐	☒ Antibodies
☐	☒ Eukaryotic cell lines
☒	☐ Palaeontology
☐	☒ Animals and other organisms
☒	☐ Human research participants
☒	☐ Clinical data

Methods

n/a	Involved in the study
☒	☐ ChIP-seq
☒	☐ Flow cytometry
☒	☐ MRI-based neuroimaging

Antibodies

Antibodies used	All unique materials are available from commercial suppliers or are available upon request from the authors.
Validation	hFANCD2 antibody was validated by western blotting with NALM-6 cell lysate. FLAG tag antibody manufacturer validated by western blot with mammalian crude cell lysates. Histidine tag antibody manufacturer validated by western blot with mammalian and non-mammalian crude cell lysates. Histone H3 antibody manufacturer validated by western blotting with K562, DAE, CTLL-2, BAEC, and C6 cell lysates. hMCM3 antibody manufacturer validated by western blotting K-562, KNRK, and NIH/3T3 whole cell lysates. hMCM4 and hMCM5 antibodies manufacturer validated by western blotting RIPA extract of HeLa cells. hNEIL3 antibody manufacturer validated by positive WB detected in HEK-293 cells, A431 cells, human skin tissue, mouse skin tissue. Phospho-hCHK1 (ser345) antibody manufacturer validated by Western blot analysis of extracts from COS cells treated with UV or MMS. hTIMELESS antibody manufacturer validated by western blotting transfected 293T cell lysates. hUbiquitin antibody manufacturer validated by western blotting with 293T whole cell lysates. hVinculin antibody manufacturer validated by western blotting on RIPA lysates of human A431 cells, lysates from chicken embryonic fibroblasts (CEF), or mouse 3T3/A31 fibroblasts. All other antibodies used in this study were validated by western blotting with Xenopus egg extracts.

Eukaryotic cell lines

Policy information about cell lines

Cell line source(s)	HAP1 cells were originally obtained from Horizon Discovery. CH12-F3 murine B lymphoma cells were a gift from M. Neuberger (MRC Laboratory of Molecular Biology) and were originally obtained from T. Honjo (Kyoto University; see Nakamura et al., Int Immunol. 1996).
Authentication	All knockouts were confirmed by PCR. Additionally, cell lines were futher validated by Western blot (NEIL3 KO) or FANCD2 ubiquitylation assay (FANCL and FANCB KO).

Mycoplasma contamination	All cell lines tested negative for mycoplasma contamination using the MycoAlert Mycoplasma Detection Kit (Lonza).
Commonly misidentified lines (See ICLAC register)	No commonly misidentified cell lines were used for this study.

Animals and other organisms

Policy information about studies involving animals; ARRIVE guidelines recommended for reporting animal research

Laboratory animals	Xenopus laevis purchased from from Nasco. Females used for egg collection were aged > 2 years. Males used for sperm chromatin preparation were aged >1 year.
Wild animals	This study did not involve wild animals.
Field-collected samples	This study did not involve samples collected from the field.
Ethics oversight	All animal work was approved by the Harvard Medical Area Standing Committee on Animals (HMA IACUC Study ID IS00000051-3, approved 10/25/2017). The institution has an approved Animal Welfare Assurance (#A3431-01) from the Office of Laboratory Animal Welfare.

Note that full information on the approval of the study protocol must also be provided in the manuscript.